Progress in Solid-State Chemistry, Vol. 10, Part 3, pp. 157–191. Pergamon Press 1975. Printed in Great Britain

MOLECULAR BEAM EPITAXY

A. Y. CHO and J. R. ARTHUR
Bell Laboratories, Murray Hill, New Jersey 07974

I. Introduction and historical background

Molecular beam epitaxy (MBE) is a term used to denote the epitaxial growth of compound semiconductor films by a process involving the reaction of one or more thermal molecular beams with a crystalline surface under ultra-high vacuum conditions. MBE is related to vacuum evaporation, but offers much improved control over the incident atomic or molecular fluxes so that sticking coefficient differences may be taken into account, and allows rapid changing of beam species. For example, using MBE it is possible to produce "superlattice" structures consisting of many alternate layers of GaAs and $Al_xGa_{1-x}As$ (Fig. 1)[1,2] with layer thickness as low as 10 Å.[3] Since electrically active impurities are added to the growing film with separate beams, the doping profile normal to the surface may be varied and controlled with a spatial resolution difficult to achieve by more conventional, faster growth techniques. Due to the increasing demand in electronic device technology for ultra-thin planar structures with precisely controlled doping profiles for use in microwave oscillators[4] and solid-state lasers,[5] there is a considerable interest in low-temperature epitaxial growth of very thin films.

The general subject of epitaxial compound semiconductor films is a broad topic which has been discussed from various aspects in a number of recent books and review articles.[6–14] Here we will be concerned only with film deposition by vacuum evaporation of the compound or its constituent elements; furthermore, the discussion will be limited largely to films of the III–V compounds because our understanding of the kinetic growth mechanism by MBE is much more complete for these materials. Both II–VI and IV–VI compound epitaxial films have been grown by MBE or related evaporation techniques and a bibliography with some representative papers on these materials is included in the Appendix.

The properties of lead and tin chalcogenide films deposited by sublimation have been extensively studied;[15] in fact PbS was probably the first compound semiconductor to be deposited by evaporation of the elements,[16] as well as the first to be grown epitaxially on a foreign substrate by this process.[16,17] However, in spite of the fact that the lead salts are rather easily grown as single crystal films,[15] little is known about the growth mechanism which is complicated by the existence in the vapor of the lead chalcogenide molecule as well as the elements.[18,19]

The III–V compounds evaporate primarily as the elements; furthermore, at temperatures where the evaporation rate is high enough for practical mass transfer, the partial pressure of the group V element is considerably greater than that of the group III element, i.e. evaporation is not "congruent". This fact would appear to cause difficulties in producing stoichiometric films, and a number of solutions to this problem were proposed by early workers. Richards *et al.*[20,21] used "flash evaporation" in which small particles of the source compound were completely vaporized on a hot tungsten ribbon, thus assuring that the vapor flux arriving at a substrate some distance away contained a stoichiometric ratio of the constituent elements. Collins *et al.*[22] used two crucibles to evaporate the constituent elements. The crucibles were placed some distance apart so that the relative flux ratio at a substrate above the crucible varied along the lateral direction between the crucibles. In this way they hoped to establish the optimum flux ratio at some position on the substrate. They were able to grow films of polycrystalline GaSb but found little effect of substrate positioning on film growth.

The "three-temperature" technique of Günther[6,23] relied on the much lower vapor pressure of the group V element over the III–V compound than over the pure group V solid. With a group V element source oven held at temperature T_1 to maintain a steady pressure in a static vacuum chamber, a group III element oven at a higher temperature T_3 providing a flux of atoms incident on the substrate, and the substrate at an intermediate temperature T_2 high enough to eliminate the condensation of excess V element on the surface, he was able to obtain stoichiometric films of a number of binary and ternary III–V compounds; however, the films were usually grown on glass substrates and were polycrystalline.

Epitaxial films of the III–V compounds were not obtained until improved vacuum conditions and clean single crystal substrates were employed. LEED studies of InSb and GaSb by Haneman[24,25] pointed out the difficulties in obtaining clean surfaces of these materials. He was able to obtain LEED patterns only after repeated use of the Farnsworth ion-bombardment-annealing technique.[26] More recently the impurities present on an etched and polished GaAs surface have been identified by Auger spectroscopy,[27,28] and the effectiveness of ion bombardment for their removal has been well established.[28] Thus, with the capability for ion bombardment and annealing of their substrates, Holloway *et al.*[29] were able to prepare homoepitaxial films of InSb up to 27 μ thick by flash evaporation. The best films exhibited X-ray rocking curves similar to bulk crystals, and Zn-diffused p–n junctions had electrical characteristics similar to diodes made from bulk material. Soon after, Davey and Pankey,[30] using the three-temperature method, grew epitaxial GaAs films on both GaAs and Ge surfaces cleaned by ion bombardment.

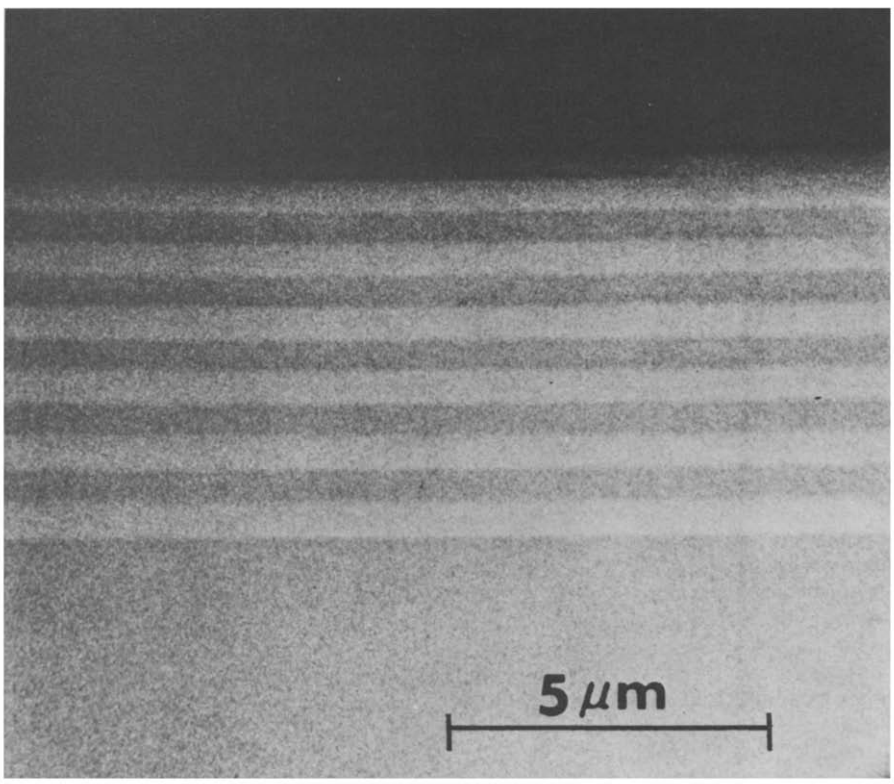

FIG. 1. A scanning electron micrograph of a cleaved section through a structure comprised of alternating 5000 Å layers of GaAs and $Al_xGa_{1-x}As$.

The use of collimated molecular beams to grow III–V compound layers was stimulated by studies of the reaction between pulsed Ga and As_2 beams incident on a GaAs surface.[31] It was found that the adsorption and desorption of Ga atoms on the polar {111} faces of GaAs obeyed a first-order rate law characterized by temperature-dependent time constants, e.g.

$$\tau_{Ga} = 2.5 \times 10^{-14} \exp \frac{2.6 \pm 0.2}{kT} \text{ sec on (111) GaAs}$$

where τ is the mean lifetime of Ga atoms on the surface. For example, at 885 K $\tau_{Ga} = 10$ sec on (111) GaAs. However, the behavior of arsenic was more complex, and depended on the surface composition. Above 500 K there was no measurable adsorption of As_2 unless Ga atoms had previously been deposited; in the latter case the sticking coefficient for As_2 was proportional to Ga coverage. This was interpreted to mean that As_2 molecules could adsorb on hot GaAs only if they collided with Ga atoms on the surface and reacted to form GaAs. This suggested that stoichiometry could be achieved by providing a sufficiently greater flux of As_2 than Ga to insure that all the Ga reacted, since the excess As_2 would not stay on the surface.

While this interpretation has since been found to be somewhat oversimplified, considerable success was achieved in growing GaAs, GaP and $GaAs_xP_{1-x}$ films on GaAs substrates[32] and on CaF_2,[33,34] and it was evident that film stoichiometry was readily attained. With the addition to the vacuum system of Auger spectroscopy for surface chemical analysis,[35,36] and reflection electron diffraction (RED) for *in situ* structural analysis,[36–39] the original uncertainties over film stoichiometry and substrate cleanliness could be resolved.

With the improved characterization of epitaxial layer and substrate resulting from the incorporation of these surface diagnostic techniques into the film growth process, the recent progress of MBE of III–V compounds has been very rapid. GaAs and $Al_xGa_{1-x}As$ layers have been grown with electrical and optical properties comparable to high quality material grown by conventional techniques. A number of device structures have been fabricated, e.g. IMPATT diodes,[117] mixer diodes,[121] double heterostructure lasers[104] and optical waveguides.[40] Other structures such as superlattice[2,3] and ultra-thin heterostructures[143] were also studied.

Since MBE is a relatively new technique whose success has been to a considerable extent dependent on improved methods of surface preparation and beam generation, in the next section we will discuss at some length the practical experimental details which have evolved so far. Section III will consider the kinetic mechanism of MBE as it is presently understood, while Section IV will discuss post-growth film evaluation methods and the results for MBE films. Section V will describe the fabrication and characteristics of some specific devices using MBE, and Section VI will discuss methods for preparing electrically isolated device structures on a single substrate—an MBE planar technology. We conclude with a description of the use of MBE to prepare structures and surfaces for research applications.

II. Experimental considerations

A. *MBE apparatus*

Figures 2 and 3 show samples of UHV systems presently used for studies of MBE. Similar systems have been described by Chang *et al.*[3,39] They are typically stainless-steel bell-jar systems, ion pumped, with normal base pressures $\sim 1 \times 10^{-10}$ torr after 8 hr bakeout or $\sim 2 \times 10^{-9}$ torr unbaked. The systems shown here are equipped with electron guns and energy analyzing optics for Auger spectroscopy and with provision for low-energy electron diffraction (LEED) and/or reflection electron diffraction (RED). Both contain quadrupole mass spectrometers for residual gas analysis and analysis of the molecular beams. The system in Fig. 2 is used primarily for studies of the detailed kinetics of molecular beam-surface interactions; consequently the mass spectrometer is mounted so that it can be moved around the substrate in order to analyze both incident and scattered beams. The system in Fig. 3 is used primarily for growing MBE layers of different compositions and dopings; it has a greater number of molecular beam sources for this purpose.

Besides improved vacuum conditions, the basic

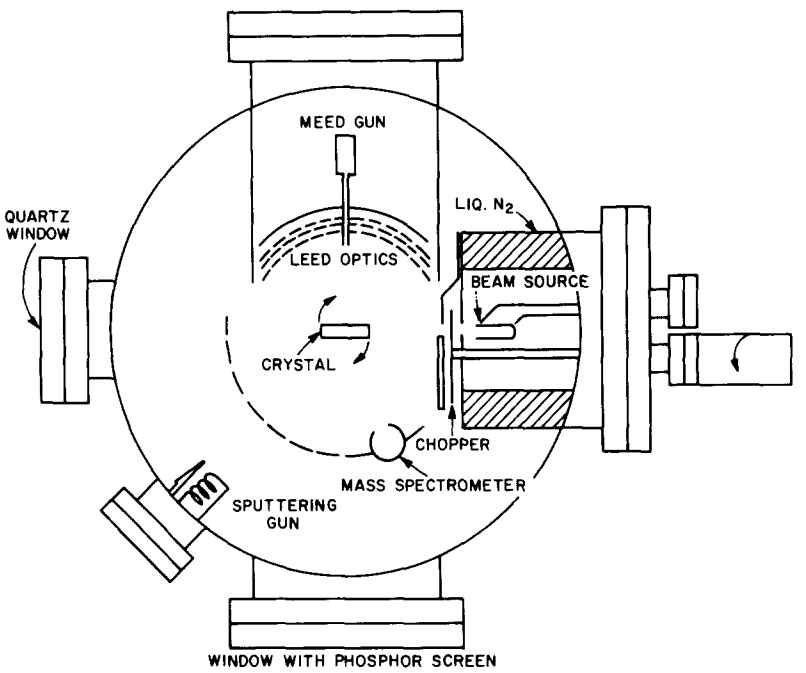

FIG. 2. Top view of MBE system used for measurement of beam reaction kinetics.

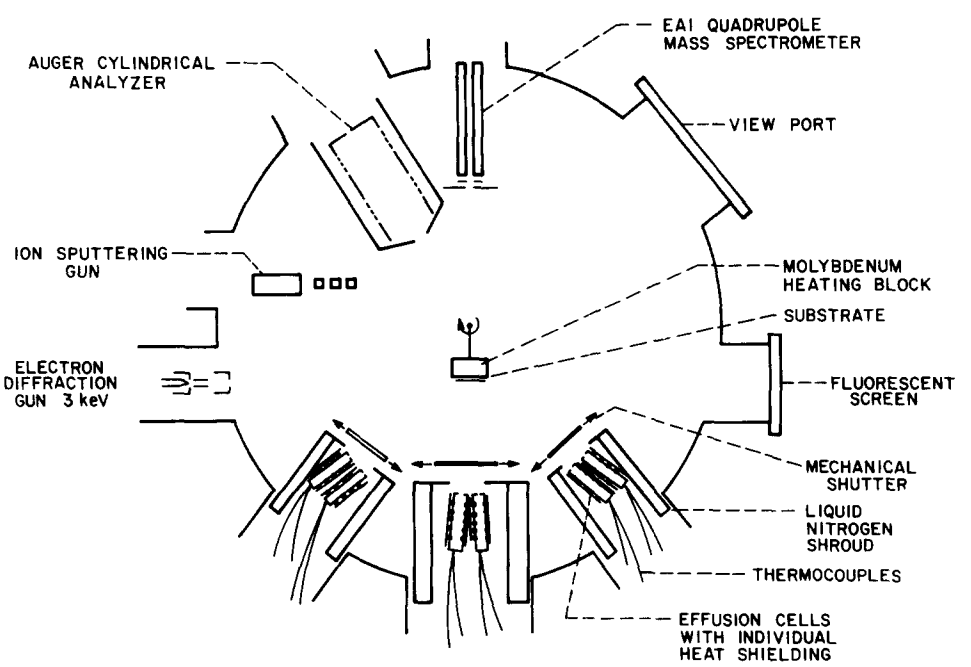

FIG. 3. Top view of MBE system used for the growth of multi-layered devices.

difference between Günther's three-temperature technique and MBE is that in the latter method all constituents are directed at the substrate as molecular or atomic beams. The beams are derived from thermal effusion cells whose temperatures are accurately controlled. In our systems, thermocouple controlled negative-feedback provides a temperature regulation of $\pm 2°$. For most elements this is equivalent to a flux regulation of $\pm 7\%$ or better.

An advantage of the MBE technique over Günther's technique is that only the source cells and the substrate are heated; this greatly reduces outgassing from the walls. Outgassing can be further reduced by providing cryogenic pumping in the form of a liquid-nitrogen-filled chamber surrounding the source ovens as shown in Figs. 2 and 3. In order to reduce the unused material flux into the chamber, a plate with beam-forming apertures is mounted on the liquid-nitrogen-cooled shroud. Finally, by means of externally controlled shutters the beams can be intercepted in order to abruptly alter the film composition. The ease of switching "on" or "off" is one of the main advantages of the use of atomic or molecular beams for growing thin films.

Ideally, the beam source should be a Knudsen cell containing vapor and condensed phase at equilibrium; in this case the flux F at the substrate is then

$$F = \frac{P_{(T)}a}{\pi L^2\sqrt{2\pi mkT}} \text{ molecule/cm}^2\,\text{sec} \qquad (1)$$

where $P_{(T)}$ is the equilibrium pressure at the cell temperature T, a is the area of the cell aperture, L is the distance to the substrate and m is the mass of the effusing species. Designs for Knudsen cell sources have been described by Foxon and coworkers.[41,42] In practice, a true Knudsen source is inconvenient because a wide aperture is needed to provide a useful rate of mass transfer and because fairly small cells are desirable in order that several may be placed in close proximity to the substrate. We have used tubular crucibles open at one end made from pyrolytic BN or high purity graphite. The crucibles are mounted within spiral Ta heater windings which are themselves enclosed within Ta foil radiation shields. These sources have the desired features of:

(a) small size ($\sim 1.5'' \times \frac{3}{4}''$),
(b) low gas evolution,
(c) rapid thermal response,
(d) low radiant power loss and uniform heating.

A requirement for the source ovens is a very low production of impurities in the molecular beam, either from outgassing or from reaction of the crucible walls with the contents. Gallium and aluminum are extremely reactive at high temperatures and reduce refractory oxides, e.g.

$$Ga_{(l)} + SiO_{2(s)} \rightarrow Ga_2O_{(v)} + SiO_{(v)}.$$

Pyrolytic BN is not measurably attacked and has a very low rate of gas evolution.

For many MBE applications the beam fluxes at the substrate must be accurately known by calibration. For GaAs films, for example, the Ga flux is determined from the film thickness since the growth rate is proportional to the Ga arrival rate.[31] The doping impurity beam fluxes are determined from the Hall measurements made on a series of layers grown on high resistivity substrates or Schottky barrier capacitance–voltage measurements on layers grown on conducting substrates (see Section IV). The arsenic flux is less critical and can be adjusted within suitable limits from observation of the RED patterns during growth (see Section II-C).

For source materials to generate the molecular beams, either pure elements (Ga, Al, As, P, Mg, Sn) or suitable compounds (GaAs, GaP, InSb) are used. The III–V compounds are useful sources of group V element molecular beams since they provide stable, well-determined beam fluxes until nearly all of the group V element is exhausted. From eqn. (1) it can be shown that for an As_2 arrival rate F at the substrate of 1–10 monolayers/sec or 10^{15}–10^{16} molecules/cm^2 sec, assuming typical geometrical factors $L \sim 5$ cm and $a = 0.5$ cm^2, $P_{(T)} \sim 10^{-2}$–10^{-3} torr in the cell. When solid GaAs is heated above 637°C,[43,44] As_2 evaporates preferentially, leaving liquid Ga on the solid surface. Thus the Ga-rich liquidus composition is quickly obtained within the cell and the partial pressures of Ga, As_2 and As_4 are given in Fig. 4.[43] As_2 pressures of 10^{-3}–10^{-2} torr in the cell are evidently obtained at 1100 K–1175 K along with Ga pressures of $\sim 2 \times 10^{-4}$–7×10^{-4} torr, corresponding to Ga fluxes at the substrate of ~ 2.5–9×10^{14} Ga/cm^2 sec or roughly $\frac{1}{3}$–1 monolayer/sec. Since the growth rate is limited by the Ga arrival, it follows that while GaAs MBE is possible using a single source containing a Ga–GaAs mixture, the growth rates obtainable are fairly low (<1 μm/hr). Consequently it is frequently desirable to include an additional source containing Ga to increase the Ga flux and growth rate.

It is worth noting that the III–V compounds used as sources provide a constant beam flux of the V element until it is nearly exhausted from the cell because the solubility of the V element in liquid III metal is quite low at normal effusion cell temperatures.[45] For example, the solubility of As in Ga at

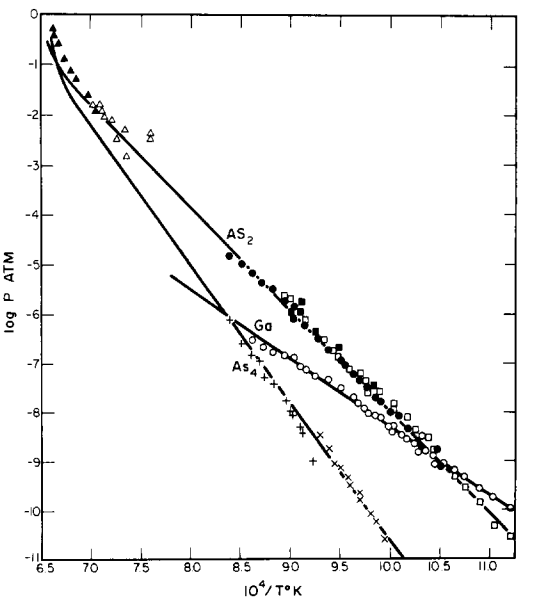

FIG. 4. Experimental measurements of the equilibrium vapor pressures of Ga, As_2 and As_4 along the Ga-rich portion of the binary Ga–As liquidus. (Ref. 43.)

1175 K is ~0.06 mole fraction,[45] so that the liquidus composition is maintained until 94% of the As from GaAs is evaporated.

It is also possible to use the pure group V element as a source along with a separate Ga source. This has two disadvantages:

1. The element, e.g. arsenic, oxidizes when the vacuum system is opened to air. Removal of this oxide requires that the source be heated to its operating temperature for some period of time prior to actual deposition. Figure 5 shows the mass spectrum observed when the As source is first heated.[46] Oxidation of the compound source is much less extensive, and only brief thermal cleaning is necessary.

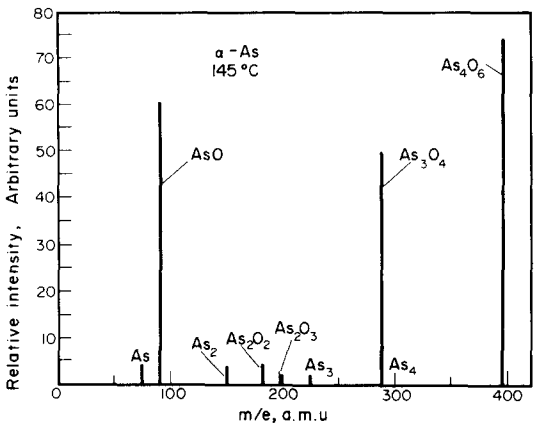

FIG. 5. Mass spectrum of oxides of arsenic observed on heating a crystalline arsenic source after exposure to atmosphere. (Courtesy of W. R. Knolle.)

2. The evaporation coefficients of elemental arsenic and phosphorous are much less than unity.[47] Consequently it is difficult to estimate the beam flux without direct measurement. In spite of these difficulties, elemental arsenic sources seem to produce somewhat purer films than do GaAs sources, and thus are useful when a low doping background is desired. Cho and Reinhart[48] observed that unintentionally doped MBE layers grown from GaAs sources had a background donor concentration N_D-N_A in the range $5-8\times10^{15}/cm^3$ while similar layers grown from an elemental As source had $N_A-N_D\approx2\times10^{14}/cm^3$. They speculated that the higher donor level was produced by Si in the source GaAs which is commonly present in undoped material at $\sim10^{16}$ Si/cm^3.

The most important requirement for the substrate holder is that it be capable of heating the substrate uniformly to temperatures up to ~650°C. This may be accomplished in a variety of ways, e.g. electron bombardment or radiant heating; however, since the substrate crystals are often thinner than 0.5 mm it is difficult to avoid lateral thermal gradients. We have found it effective to mount the substrate wafer on an internally heated Mo block, using a thin layer of Ga or In between the block and crystal to provide good thermal contact without the necessity for rigid clamping. The difference in thermal expansion between block and substrate can introduce strain and generate dislocations in the growing film if the substrate is tightly mounted. The metal layer (which is molten at the growth temperature) provides good enough heat transfer that there is no optically measurable difference in temperature between the block and substrate. As long as reasonable care is taken to restrict the metal initially to the back of the substrate, there is no indication from either Auger spectra or scanning electron microscopy that any surface diffusion onto the growing surface occurs. There are two limitations to the use of a liquid metal layer under the substrate:

1. In has an appreciable vapor pressure above 550°C and is gradually lost by evaporation;
2. Ga has a lower vapor pressure but is highly reactive at high temperatures, causing gradual erosion of the Mo block after prolonged use at 550–600°C.

B. *Substrate preparation and surface contamination*

The introduction of Auger electron spectroscopy (AES) as a tool for surface chemical analysis has taken most of the guesswork out of substrate preparation. AES is an energy analysis of the secondary electrons emitted by a surface which is bombarded by a primary electron beam of 3–5 keV energy. Ionized core levels which are generated in surface atoms by the primary beam can be filled from higher levels by a two-electron Auger process in which one electron may gain sufficient energy to leave the crystal. From a secondary electron energy spectrum such as shown in Fig. 6 information about the number and chemical identity of atoms undergoing the Auger recombination may be determined from the intensity and energy of the peaks. The signal intensity as a function of distance into the crystal is determined largely by the escape depth of the excited Auger electrons, and for peaks between 50 and 1000 eV the signal is obtained almost entirely from the first one or two atoms layers. Thus AES is obviously of great importance to surface studies; it has been discussed in detail in a number of recent reviews.[49–51]

For implementing AES, an electron gun capable of furnishing a focused beam of 25–100 μA at 3–5 keV is needed along with electron energy analyzing optics. Two analyzing schemes are in common use, the retarding grid LEED-Auger optics used in the system shown in Fig. 2 and the cylindrical mirror analyzer (CMA) in the system in Fig. 3. Each has certain advantages for use in MBE.

The retarding grid analyzer is a high-pass filter; consequently the total current reaching the collector can be relatively large producing a larger shot-noise than that in the CMA which is a band-pass analyzer. The noise from the retarding grid analyzer can be reduced by filtering but at a sacrifice in response speed (scan rate). On the other hand, the retarding grid system has a long focal length, typically several inches, so the analyzer can be physically distant from the substrate, minimizing to some extent contamination of the grids from the source beams. The CMA, however, is usually designed with a short focal length, <1 cm, so that either motion of the sample holder or analyzer is necessary to keep the analyzer away from the crystal and out of the direct beams during growth.

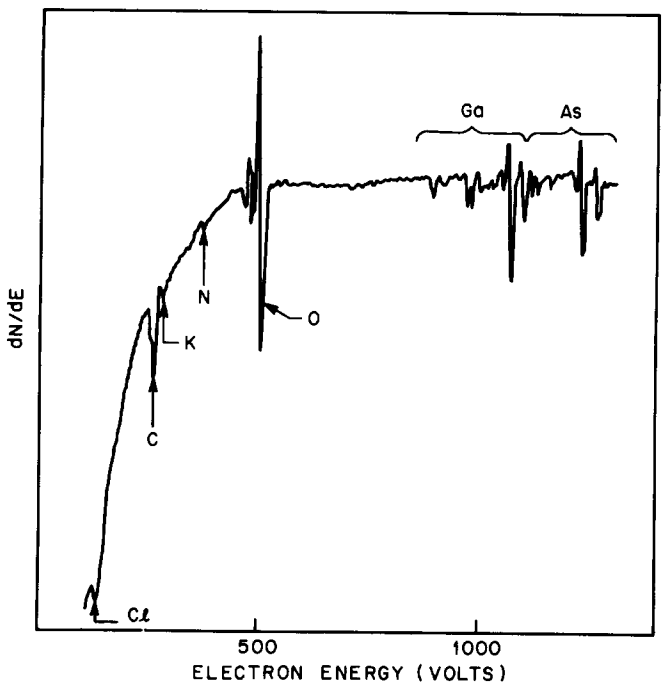

FIG. 6. Auger spectrum of unpassivated Br–methanol etched GaAs using a hemispherical grid LEED/Auger analyzer.

With either analyzer some type of shutter in front of the entrance is desirable during the growth process to avoid the buildup of insulating deposits within the analyzer. Thus while it is possible to operate the Auger spectrometer during growth, it is impractical to do so for very long, and spectra are usually taken with molecular beams off and the substrate at room temperature.

The sensitivity of AES for a given element depends on a number of factors, e.g. distribution on the surface or in depth, presence of interfering elements, instrumental effects such as primary beam current and energy and spectrometer resolution; however, for uniformly distributed surface layers the sensitivity is typically 0.1% of a monolayer for most elements. Since the normal concentration of intentionally added doping impurities in GaAs is much less than 0.1%, AES is not particularly useful for measuring bulk dopant concentrations.

AES has been of most use in MBE studies for characterizing the initial substrate surface. Figure 6 shows the Auger spectrum of an uncleaned GaAs substrate after a typical chemical etch-polish in 5% Br-methanol, methanol and water rinse and 8 hr backout of the vacuum system at 250°C. Large peaks due to surface C and O are indicated as well as the complex high energy structure due to Ga and As. This spectrum was taken with a retarding grid analyzer.

The relative surface concentrations of C and O obtained from the ratio of the 270 V C and 510 V O Auger peak heights for chemically etched GaAs depend strongly on the exact etching procedure. In particular, it is possible to enhance the oxygen content and reduce the carbon content by flushing the etching solution away from the crystal with water before the surface is exposed to air. GaAs surfaces passivated in this manner are relatively stable to laboratory air and do not adsorb carbon readily. This is important because oxygen can be removed by heating GaAs in vacuum to 525–535°C[35,48,52] while carbon is hardly affected by heating. Figure 7 shows Auger spectra taken with a CMA of an oxygen-passivated surface before and after heating. It can be seen that heat treatment

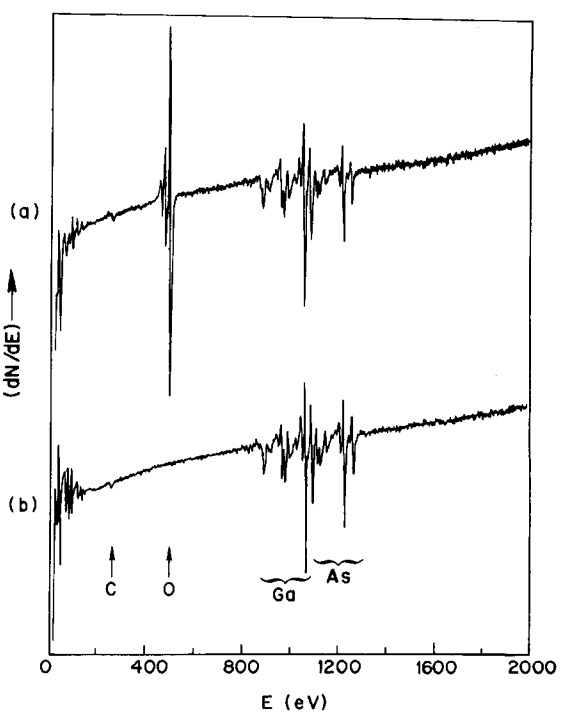

FIG. 7. Auger spectrum of (100) GaAs using CMA: (a) etched in Br_2–methanol and rinsed in deionized water, (b) after heating in vacuum to 530°C.

alone was sufficient to produce a nearly clean surface with only a few percent of a monolayer of carbon remaining. Carbon contamination at this low level does not have any noticeable effect on epitaxial growth, and is quickly covered by the growing film.

Carbon contamination in excess of about 20% of a monolayer damages the film quality by causing surface facetting and twinned growth. The microscopic appearance of the surface after growth on a carbon contaminated substrate (Fig. 8) suggests that growth in this case occurs by a nucleation process, just as observed for Si by Joyce and coworkers.[53,54] While careful chemical treatment of the substrates can usually keep the carbon below this level, the surface contamination is somewhat variable from sample to sample, and since heat treatment is not effective in carbon removal it is desirable to have some provision for ion-bombardment cleaning in the vacuum system.[25,28] On a flat, etch-polished surface of GaAs, the removal of 4–8 atom layers by ion bombardment is usually sufficient to remove all contamination detectable by AES; furthermore, there is rarely any evidence for out-diffusion of impurities upon subsequent annealing.

The general procedure for GaAs substrate preparation uses the lapping and chemomechanical polishing methods described by Jensen,[55] who lists several polishing solutions which are effective. After a suitably oriented GaAs wafer has been etch-polished to remove all surface damage and leave a mirror finish, the crystal is flooded with water to stop the etching and passivate the surface with oxide. The crystal is blown dry with filtered N_2 or freon and placed on the substrate holder which is warmed sufficiently to melt the Ga or In metal layer under the crystal. The surface tension of the molten metal is sufficient to hold the sample on the heating block, but thin Ta wire clips are also used occasionally to prevent any sliding. Care is taken to avoid mounting the crystal rigidly. All operations in air are carried out under dust-free conditions. The sample holder is installed in the vacuum system as soon as possible after polishing mainly to avoid particulate contamination. In a vacuum of $\sim 10^{-9}$ torr a properly passivated surface can be cleaned by heating to 540°C for ~1 min. If some carbon remains, a few minutes Ar^+ bombardment will usually remove it, leaving the surface clean but disordered. Annealing the ion-bombarded surface to ~350°C briefly usually produces a flat, well-ordered surface as indicated by RED.

Recontamination of cleaned III–V compound surfaces by adsorption of background gas is usually not a problem at pressures below 10^{-9} torr. With the possible exception of surfaces of the Al compounds, sticking coefficients of most gases are quite low on these materials, $< 10^{-3}$.[52,56] However, just as in the case of Si,[57] an electron beam of a few keV energy incident on the surface of GaAs or $Al_xGa_{1-x}As$ can greatly enhance the contamination rate for both oxygen and carbon. To minimize this effect, neither the Auger spectrometer nor the RED gun should be extensively used when the background pressure of reactive gases is much greater than $\sim 1 \times 10^{-9}$ torr.

A further refinement of AES is the analysis of composition as a function of depth into the crystal, using ion bombardment to slowly remove the surface layers.[51] Ludeke *et al.*[58] have used AES sputter-profiling to examine GaAs–$Al_{0.25}Ga_{0.75}As$ periodic structures ("superlattices") grown by MBE. The alternating layers were 50 Å thick. While the expected periodic variation in the Al Auger peak was observed, the amplitude of this variation decreased with depth into the crystal. This was attributed to a lack of uniformity of the sputtered crater across the area sampled by the Auger beam. Their results point out the present limitations in high-resolution depth analysis of layered structures.

C. *Electron diffraction and surface structures*

The use of reflection electron diffraction techniques to observe changes in the structure of the

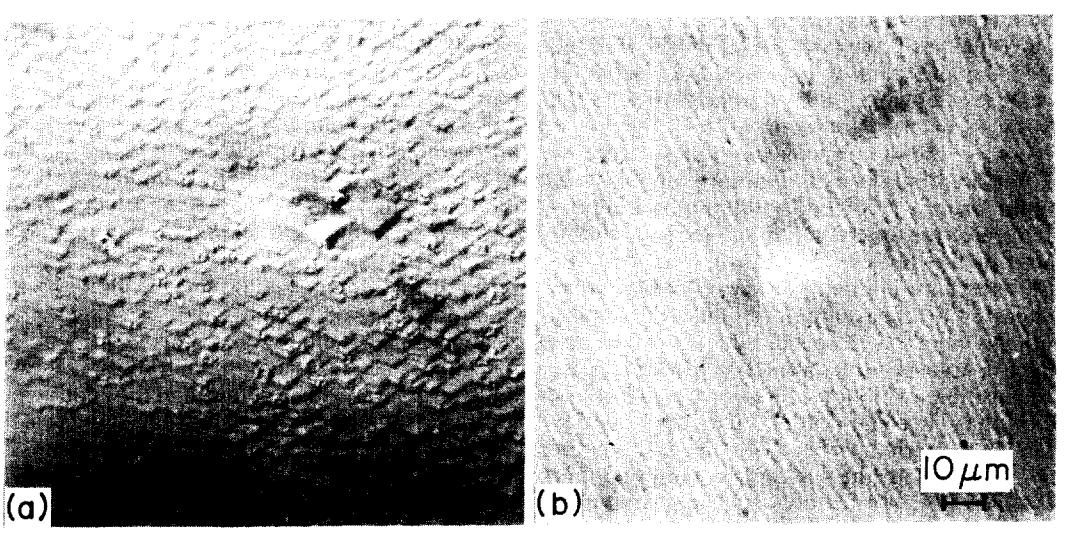

FIG. 8. Optical micrograph (500×) of the surface of ($\bar{1}\bar{1}\bar{1}$) GaAs with 5000 Å MBE layer. (a) Region of surface with initial C contamination of ~0.2 monolayer. (b) Region of surface with initial C contamination <0.1 monolayer.

outermost layer of atoms in a crystal during growth has played an extremely important role in the development of MBE technology.[37] RED has been important because it is a very sensitive yet simple diagnostic tool which can easily be used while the film is growing and because certain of the bulk properties of GaAs have been found to depend significantly on the surface structure present during MBE.[59] It must be admitted that the exact atomic arrangement of the surface is not known with certainty for any III–V compound; with the possible exception of the {110} cleavage planes, the clean III–V surfaces are reconstructed with a different translational symmetry than that of the bulk lattice.[24,25,60,61] RED is used qualitatively to detect changes in the surface symmetry.

While most previous studies of III–V surface structure have been made using normal incidence LEED,[24,25,56,60–63] it is experimentally more convenient to use glancing incidence RED during MBE because this geometry allows the molecular beams to be directed normal to the surface while the diffraction pattern is observed. Also, RED can detect polycrystalline structures. Both LEED and RED have a comparable surface sensitivity because the penetration depth of the incident electron beam depends on the energy component normal to the surface. In either case this is ~50–150 eV even though the total energy of the RED beam is 3–50 keV. RED and LEED are sensitive to only the first few atomic layers of a crystal because the probability for inelastic scattering is very high for electrons in the energy range ~50–150 eV, so that only those electrons which are elastically scattered very near the surface are able to escape without energy loss.

The use of RED and LEED to obtain surface structural information has been discussed in detail in a number of review articles.[63–67] While a complete structure analysis is quite complex, the symmetry and dimensions of the reciprocal lattice may be determined very easily by either technique. In addition RED provides considerable information about surface topography, with characteristic diffraction features indicating the presence of microscopic roughness, twinning, or oriented inclined facets on an otherwise flat surface. Information of this nature is obviously of value in studies of the early stages of crystal growth.

Figure 9 shows high energy RED patterns (40 keV with primary electron beam along the [$\bar{1}\bar{1}0$] azimuth) from a (100) GaAs surface and corresponding electron micrographs of Pt-shadowed C replicas of the surface.[68] It can be seen that the initial, thermally cleaned surface is rough which produces a diffraction pattern of spots; the electron beam can penetrate the surface asperities and produce a transmission diffraction pattern. After the deposition of 150 Å of GaAs by MBE, the surface has become flatter and the electron diffraction pattern has become elongated in the direction normal to the surface. At the same time additional diffraction features have appeared halfway between the original columns of diffraction spots. After growth of 1 μm of GaAs the surface appears completely flat and featureless while the diffraction pattern is uniformly streaked normal to the crystal surface. This is due to a relaxation of the Laue condition in the direction along the surface normal because the high attenuation of the beam into the crystal means that the diffracted beams are sampling effectively only a two-dimensional crystal. Streaking is also enhanced by refraction of the electron beam as it crosses the interface at low angles. Both of these effects depend on the angle at which the electron beam strikes the crystal, and thus are a measure of the microscopic roughness when the macroscopic angle of incidence is fixed at ~1° as in the figure. If additional surfaces inclined to the macroscopic surface were to form by thermal facetting or three-dimensional nucleation, diffraction streaking perpendicular to these surfaces would indicate their presence.[70]

The additional diffraction features ("$\frac{1}{2}$-order" streaks) which appear in Figs. 9b and 9c are due to the formation of a reconstructed surface structure which has twice the unit mesh length as the unreconstructed surface.† One of the most interesting observations in the development of MBE has been the multiplicity of surface structures on all but the {110} cleavage planes of the III–V compounds. Jona[60] first observed GaAs (100)–6 and GaAs (100)–C(2 × 8) structures on a sputtered and annealed surface using LEED, but found them difficult to reproduce systematically. Cho[37] found on epitaxial surfaces that the existence of these structures as well as that of the GaAs (100)–C(8 × 2) depended on the crystal temperature and the arrival rates of Ga and As at the surface. Figure 10 shows diffraction patterns from the GaAs (100)–C(2 × 8) structure obtained by growth under conditions similar to those used in preparing the surface for Fig. 9; however, diffraction in three azimuthal directions is shown. Unlike LEED, a RED pattern does not show the entire translational symmetry of the surface; it is necessary to obtain patterns at different azimuths. From these patterns, a map of the reciprocal lattice symmetry can be drawn as in Fig. 10d.

Such a large unit mesh is beyond our present capabilities for detailed analysis. To indicate further the complexity of the situation, five additional structures have been observed on (100) GaAs.[37,39] Some of these structures are observed only at elevated temperatures within a narrow range of incident Ga and As_2 fluxes; however, there are two principal structures stable over a fairly wide range of temperatures and fluxes. These are the GaAs (100)–C(2 × 8) in Fig. 10 and (100)–C(8 × 2). A temperature-flux ratio "phase diagram" is shown in Fig. 11 where the C(8 × 2) structure is referred to as "Ga-stabilized" and the C(2 × 8) is referred to as "As-stabilized" because of the relative flux conditions necessary for their existence. While a discussion of the transition between these structures will be deferred to the next section, the results shown in Fig. 11 strongly suggest that the structural changes involve the gain or loss of the more volatile constituent arsenic from the surface, i.e. changing surface composition.

Dual surface structures are also found on the

†Following Wood,[69] we use the term "unit mesh" as the 2-D analog of "unit cell".

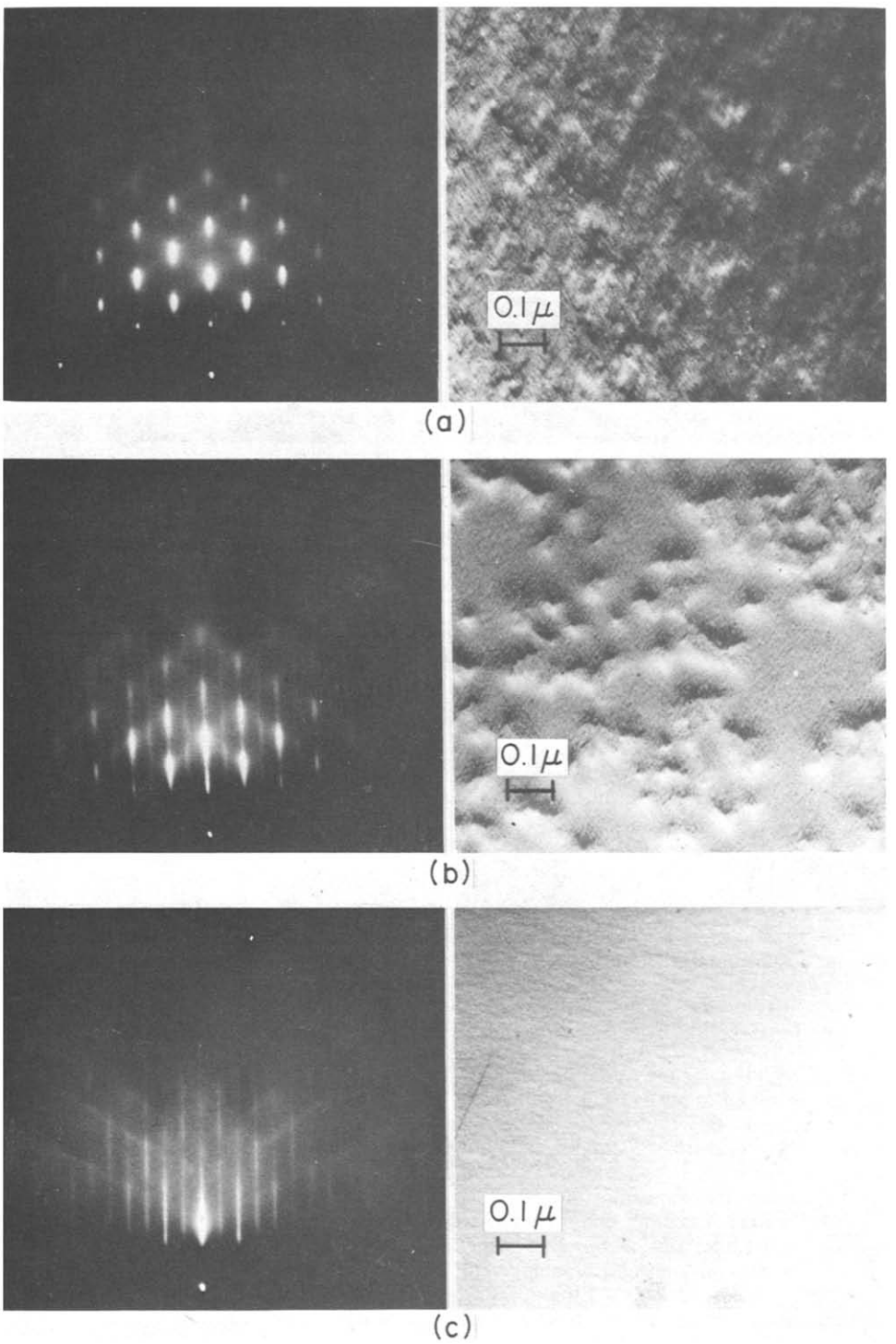

FIG. 9. RED patterns (40 keV, $\bar{1}\bar{1}0$ azimuth) and the corresponding electron micrographs (38,400×) of Pt–C replicas of the same surface. (a) Br_2–methanol polish-etched GaAs heated in vacuum to 580°C for 5 min. (b) 150 Å layer of GaAs deposited on surface of (a). (c) 1 μm GaAs deposited on surface of (a). (Ref. 68.)

{111} planes of GaAs and GaP.[1,70] On the $(\bar{1}\bar{1}\bar{1})$–B surface the arsenic or phosphorus-stabilized structure is $(\bar{1}\bar{1}\bar{1})$–2, while the gallium-stabilized structure is a complicated $(\bar{1}\bar{1}\bar{1})$–$\sqrt{19}$ – 23.4°. On the (111)–A surfaces only (111)–2 was observed by RED[59] regardless of the As_2/Ga ratio or substrate temperature during MBE. However, varying the ratio of As_2/Ga does produce different intensities in the half-order diffracted beams observed by LEED[71] suggesting that there may be two structures on this surface as well. All of these structures have been examined by Auger spectroscopy and no evidence of any impurities has been observed. All the GaAs spectra compare well with those obtained

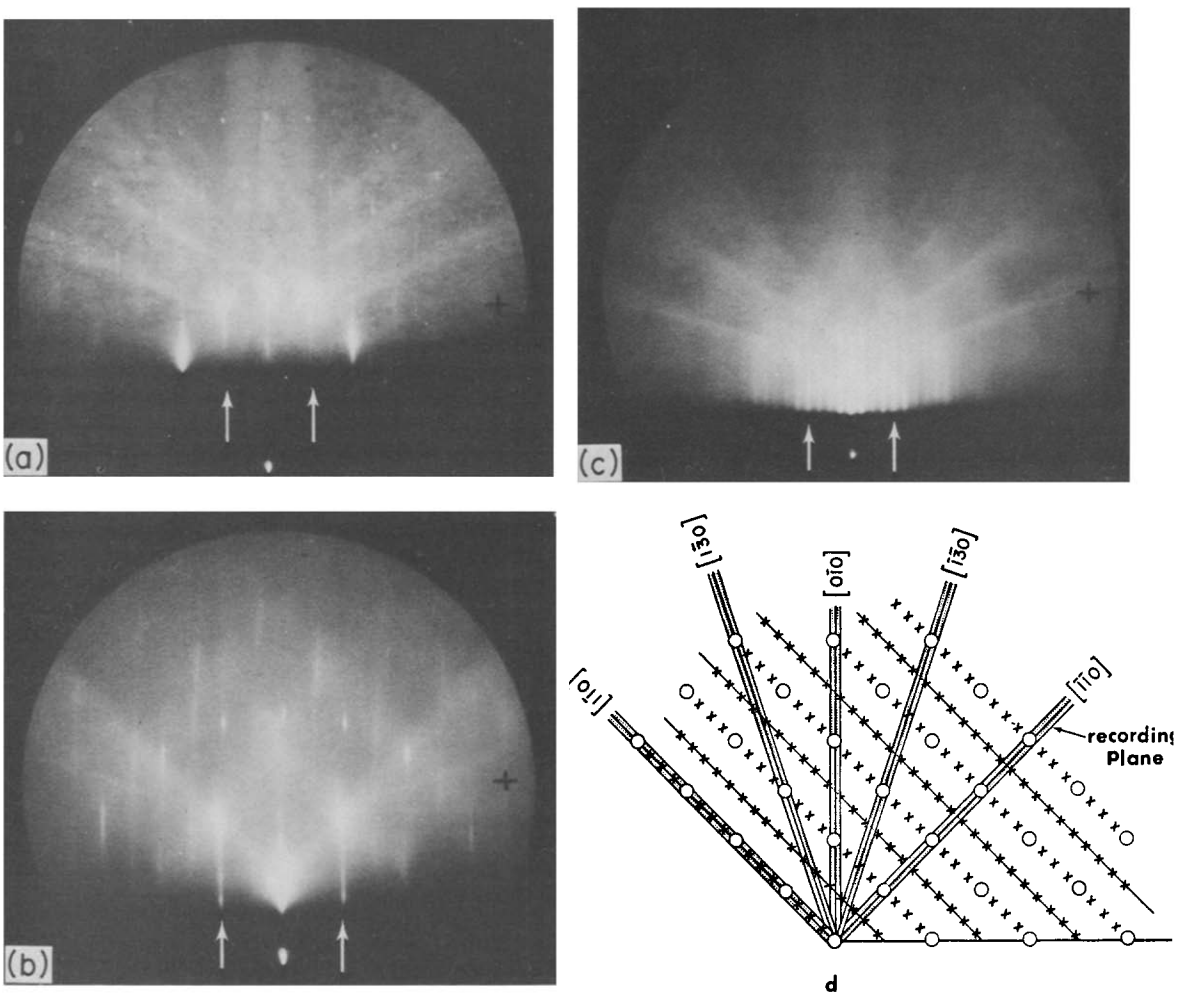

FIG. 10. RED patterns from various azimuths during MBE of GaAs on (100) plane. The arrows indicate location of bulk diffraction features. (100)C–(2 × 8)–As. (a) [1$\bar{1}$0] azimuth. (b) [0$\bar{1}$0]. (c) [1$\bar{1}$0]. (d) Schematic of the reciprocal surface net obtained from the diffraction patterns. Open circles represent unreconstructed (or bulk) net points; crosses represent points on the reconstructed reciprocal net. (Ref. 37.)

by Uebbing and Taylor[72] from cleaved[110] surfaces. Thus stabilization by an impurity, which has been reported to produce the Ni stabilized Si(111)–$\sqrt{19}$ – 23.4° structure,[73,74] can be ruled out in these cases. Mark and coworkers[75,76] have proposed that reconstruction occurs on the {111} surfaces of III–V and II–VI compounds because of the partial ionic character of the bonding. They concluded that the loss or gain of $\frac{1}{4}$ monolayer of one component is necessary to avoid the build-up of a large potential due to the bulk dipole field along the polar axis, and they showed that structural models could be generated which satisfy the $\frac{1}{4}$ monolayer criterion and have the same symmetry as all of the observed {111} structures. Their models are also consistent with the experimental observation that arsenic is in fact lost or gained by the GaAs surface when transformations between the structures occur, as would be expected from Fig. 11.

In spite of the apparent complexity of surface structures on the III–V compounds and our inability so far to solve any of them, we emphasize that the diffraction patterns generated by them are highly reproducible for given ambient conditions of flux and temperature. Thus reflection diffraction serves as an invaluable means of characterizing the surface during the growth process.

An additional feature of RED is that the equipment can be quite inexpensive. In the two systems shown in Figs. 2 and 3, the electron beam is obtained from the medium energy electron gun (1.5–3 keV).[77] With these energies the scattering angles are relatively large, so that a suitable camera length is obtained with a fluorescent screen mounted ~15 cm from the crystal. With the screen close to the crystal and source beams there is some problem with the gradual buildup of As layers and reduction of light output unless a movable shutter is used to cover the screen except when the RED system is operating.

Some definite improvement in beam focusing and diffraction spot size is obtained using high-energy electrons (35–50 keV). The long camera length (~1 m) required places the phosphor screen far enough from the molecular beams that contamination of the screen is not a problem. For quantitative RED measurements Dove *et al.*[78] and Chang *et al.*[3] have described a scanning high-energy system in

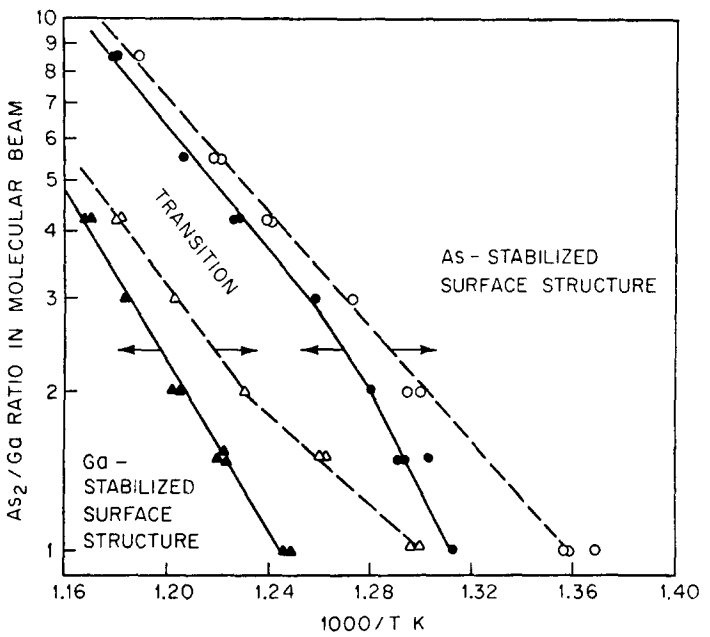

FIG. 11. As_2/Ga molecular beam flux ratio as a function of substrate temperature when the transition between As-stabilized and Ga-stabilized structures occurs. Since there is hysteresis in the transitions, depending on whether the substrate temperature is increasing or decreasing, two sets of curves are shown. (Ref. 68.)

which the diffracted beams are magnetically scanned over a current collector to provide a graphical record of beam intensity.

III. Mechanism of MBE

A. *Growth process*

Our understanding of the growth process has been gained primarily from studies of growth rate, surface morphology and reaction kinetics. Although the studies have been made almost entirely on GaAs, the fact that epitaxial layers of GaP, AlAs, InP and InSb as well as the mixed crystals $GaAs_xP_{1-x}$, $Al_xGa_{1-x}As$, and $Ga_xIn_{1-x}As$ have all been grown under conditions similar implies that the growth process is not markedly different for most of the III–V compounds.

The surface morphology of GaAs MBE films has been studied by combined RED and electron microscopy of surface replicas as mentioned in the previous section. Some of the surface replicas were made by *in situ* shadowing with Pt followed by evaporation of a carbon support layer.[70] Abbink *et al.*[79] used this technique to demonstrate that evaporated Si films grew by the addition of atoms to step edges with consequent migration of steps across the surface.[80] The $(\bar{1}\bar{1}\bar{1})$ GaAs growth surfaces also showed the presence of linear arrays of steps ~25 Å high perpendicular to the $[\bar{1}\bar{1}2]$ direction.[70] A step-growth model is consistent with the results shown in Fig. 9 in which the surface became flatter as growth continued, since surface asperities should be excellent step sources. As shown by Burton *et al.*[80] the effective repulsion between steps and acceleration of steps away from such a source result in flattening, i.e. a reduction in step density. While *in situ* replication experiments have not been carried out on (100) surfaces, the RED patterns show a similar smoothing with growth.[37]

Nucleated growth has been observed, as mentioned in Section II; however, nuclei are always associated with a high surface impurity concentration or mechanical damage or both.[73] There is some orientation dependence on the tendency for nucleation. The $(\bar{1}\bar{1}\bar{1})$–B face of GaAs is more likely than the (100) to form nuclei during growth under comparable conditions. The carbon contaminated $(\bar{1}\bar{1}\bar{1})$ surface also has a pronounced tendency to form [110]-sided facets when heated above 500°C,[27,81] while the clean $(\bar{1}\bar{1}\bar{1})$ and (100) and (111) surfaces are relatively stable at this temperature.

The kinetics of the reaction of Ga and As_2 molecular beams incident on a GaAs surface have been investigated by modulated beam mass spectrometry.[31,81] In these experiments the incident Ga and As_2 beams were modulated by a rotating chopper wheel prior to arrival on the GaAs substrate. A mass spectrometer viewing the substrate as shown in Fig. 2 was used to measure the desorption rate as a function of the varying surface population of ad-atoms. Experiments of this type have become a powerful way to study adsorption on both metals[82-85] and semiconductors[31,86,87] because they provide a direct measurement of the adsorption lifetime or mean residence time of atoms on a surface. For a first-order desorption process the surface lifetime τ, the ad-atom concentration n and the desorption rate Γ are related by

$$\Gamma = n/\tau. \tag{4}$$

If now a beam of atoms of intensity F is suddenly incident on the surface, the rate of change of n is

$$\dot{n} = -n/\tau + F. \tag{5}$$

With the initial condition $n(0) = 0$ and the assumption that $\tau \neq f(n)$, eqn. (5) can be integrated, and from eqn. (4),

$$\Gamma(t) = F(1 - e^{-t/\tau}). \quad (6)$$

In a similar manner it can be shown that when the beam is shut off abruptly, the desorption rate will decay as $e^{-t/\tau}$. These simple predictions are closely followed by Ga on GaAs as shown in Fig. 12, and from the temperature dependence of τ the activation energy, E_d, for desorption may be determined,

$$\tau = \tau_0 \exp(E_d/RT). \quad (7)$$

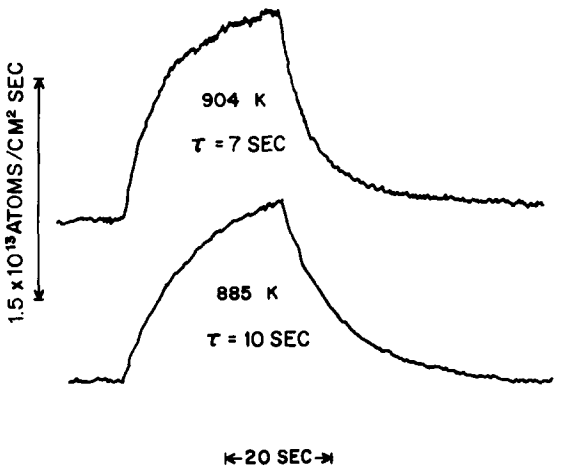

FIG. 12. Desorbed pulse shape from an incident rectangular pulse of Ga on (111) GaAs at two temperatures.

As_2 molecules on GaAs do not desorb according to eqn. (6). Figure 13 shows the desorbed As_2 flux from GaAs on which a periodically interrupted beam of As_2 was incident. The first two desorption pulses in the figure suggest that the surface lifetime of As_2 on clean, heated GaAs is very short; however, the third pulse indicates that on Ga-covered GaAs there is an appreciable lifetime, with desorption of As_2 increasing only as the available Ga is consumed. These observations led to the original proposal that adsorbed Ga is necessary for As_2 to adsorb on GaAs at elevated temperatures.[31]

More recent experiments of the same type have shown that As_2 has a brief but finite lifetime on clean GaAs above 250°C, implying a binding energy of ~0.38 eV for the molecule.[41] Furthermore, reaction of As_2 with the surface can occur even without excess Ga provided that the initial GaAs surface has the "Ga-stabilized" surface structure described in the previous section.[81] Approximately one-half monolayer of arsenic atoms can be incorporated into the surface at 550°C, upon which the surface structure becomes "As-stabilized". If the As_2 beam is shut off, the surface reverts back to the Ga-stabilized structure with the evolution of $\sim 1.8 \times 10^{14}$ As_2 molecules/cm^2 ($\sim\frac{1}{2}$ monolayer of atoms).

The observations are consistent with a model in which As_2 molecules are first adsorbed into a mobile, weakly-bound precursor state. Dissociation of adsorbed As_2 can occur when the molecules encounter paired, empty As sites. At elevated temperatures recombination of As atoms to molecules and subsequent desorption is also possible. This model can be expressed by the reaction sequence

$$As_{2(g)} \rightleftarrows As_2^* \quad (8)$$

$$As_2^* + 2V^*_{(As)} \rightleftarrows 2As^*_{(As)} \quad (9)$$

where the asterisks denote surface species. It can be shown that for this reaction sequence the sticking coefficient for As_2 is given by[81]

$$S = \frac{k\tau(1-\theta)^2}{1 + k\tau(1-\theta)^2} \quad (10)$$

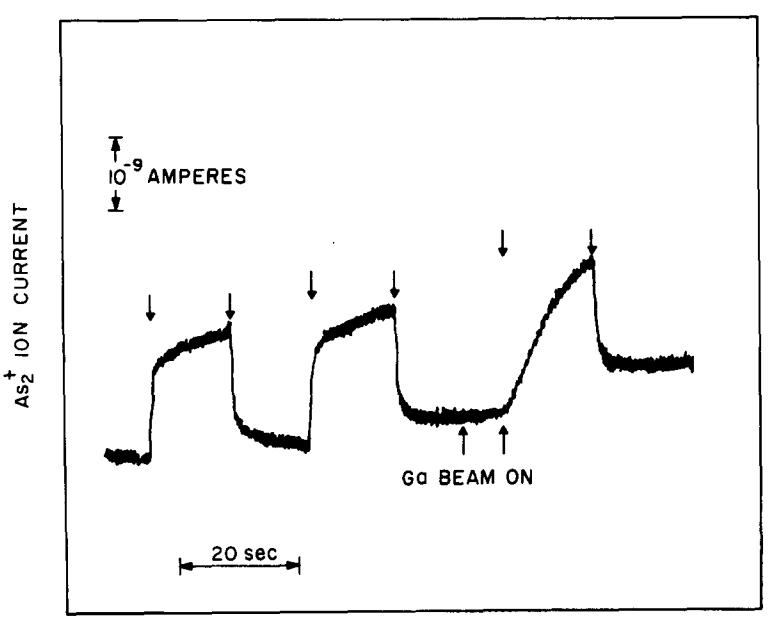

FIG. 13. Desorbed pulse shapes from incident rectangular pulses of As_2 on (111) GaAs; prior to third As_2 pulse ~0.5 monolayer Ga was deposited during indicated period.

where τ is the surface lifetime of As_2^* and k is the rate constant for dissociation. θ is the fractional coverage of dissociated arsenic. From a fit of the experimental modulated beam results to this kinetic model it was found that the Ga-stabilized structure is obtained with $\theta < 0.1$ while the As-stabilized structure is obtained when $0.5 < \theta < 0.6$.

Thus the RED patterns do in fact characterize surfaces with a considerable variation in composition. This can be quite important during MBE since it has been found that the photoluminescent efficiency of undoped films depends on the surface structure present during growth.[59] Films grown with the Ga-stabilized structure are about five times more efficient than those grown with the As-stabilized structure. Evidently the native defect concentration is altered by the different growth conditions. Also it has been found that the carrier type of films doped with the amphoteric impurity Ge depend on growth conditions.[88] Ge codeposited on a surface with $\theta_{As} < 0.1$ (Ga-stabilized) will encounter a preponderance of As sites on which Ge acts as an acceptor, while if $\theta_{As} > 0.5$ (As-stabilized) the excess of Ga sites available for Ge produces a surplus of donors. It is significant that the n-type films grown with the As-stabilized surface are found to be compensated, which is consistent with $\theta_{As} \sim 0.5$ since then both As and Ga sites are present.

From the general growth mechanism discussed above it would be expected that the growth rate of MBE GaAs would be limited entirely by the Ga flux F_{Ga} incident on the substrate, i.e.

$$R = \alpha F_{Ga} \tag{11}$$

where for F_{Ga} in atoms/cm^2 sec and R in μm/hr, $\alpha = (6.18 \times 10^{14})^{-1}$. While the growth rate can be accurately measured from micrographs of the film thickness, the Ga flux can be measured with the mass spectrometer only with an absolute accuracy of $\pm 50\%$. Equation (11) would be inaccurate only if some Ga incident on the crystal could desorb prior to reaction. While Ga can be detected leaving the substrate above 600°C with *no* As_2 arriving, the desorbing Ga flux disappears when a ten-fold excess flux of As_2 is incident.[89] Thus it is concluded that eqn. (11) is correct and provides an accurate means for calibrating the group III-element flux.

B. *Doping*

For the fabrication of devices by MBE, the ability to add controlled amounts of electrically active impurities is an important consideration. Unfortunately this aspect of MBE is not well understood at present, although a number of suitable impurities have been used to grow films with both n- and p-type conductivities. The difficulty in trying to predict which elements will be suitable for MBE is that the doping process necessarily involves both the adsorption of the impurity on the surface and its subsequent incorporation into the bulk as the film grows. There are few published results which are relevant to these processes on III–V compounds, so that each potential dopant must be tested empirically.

Since so little is yet understood about the mechanism of dopant incorporation, in this section we will simply describe briefly the behavior of those elements which have been used successfully. It is convenient to divide them into two classes, those which are strongly adsorbed and those for which the sticking coefficient, S, is less than unity at the growth temperature.

(a) $S = 1$

Si.[90] Silicon in GaAs is an amphoteric impurity. For GaAs grown by liquid-phase epitaxy, Si-doped layers are heavily doped and closely compensated. However, for GaAs grown by MBE the Si-donor dominates and close compensation is not observed. Concentrations of 1×10^{16} to 5×10^{18}/cm^3 have been readily obtained. Useful doping fluxes of 10^{11} atoms/cm^2 sec or less are conveniently obtained by sublimation.

Ge.[88] As we have mentioned, Ge acts as an amphoteric dopant in MBE GaAs. If the growth conditions are such that the Ga-stabilized surface structures are obtained, the resulting Ge-doped film is p-type, while if the As-stabilized structures are present during growth the film is n-type. Thus p–n junctions can be grown by simply varying the As_2 flux. Ge concentrations as high as 5×10^{18}/cm^3 have been obtained.

Sn.[68,91] Sn is a very convenient n-type dopant for both GaAs and $Al_xGa_{1-x}As$. Doping concentrations as high as 1.2×10^{19}/cm^3 have been obtained, while Hall mobility measurements indicate that between 1×10^{17} and 1×10^{18}/cm^3 there is very little compensation occurring in Sn-doped GaAs. Cho has recently observed that Sn has a tendency to segregate at the growth surface, producing doping profiles which are not as sharp as those obtained using Si or Ge.[92]

Mn.[93] Mn was first detected by photoluminescence as a residual acceptor impurity in MBE GaAs, possibly derived from stainless-steel rods used to support the effusion cells in their experiment. When Mn is used as an intentional dopant, the resulting acceptor concentration depends on the surface stoichiometry during growth. The highest acceptor concentration obtained so far is 1×10^{18}/cm^3 in a film grown under As-rich conditions.

Te.[81,89] Te, an n-type dopant in GaAs, has a high vapor pressure, roughly comparable to that of Zn, and might be expected to be similarly difficult to incorporate in MBE GaAs. However, Arthur observed that a Te_2 beam reacted strongly with GaAs at 500°C and in fact displaced the outer layer of arsenic atoms from the As-stabilized structure, as shown in Fig. 14. Little arsenic was desorbed from the Ga-stabilized structure when Te_2 was incident. Auger spectroscopy revealed that after exposure to the Te_2-beam both surfaces contained a large amount of Te ($0.5 < \theta < 1$) which could not be thermally desorbed up to 650°C. When a GaAs crystal with a Te-stabilized surface was exposed to Ga and As_2 beams, film growth occurred; however, the Te layer remained on the surface. While subsequent analysis of the film indicated that doping with Te had occurred to an extent of $\sim 10^{19}$ Te/cm^3, the surface concentration of Te remained near a monolayer even though no Te_2 beam was arriving.

Thus Te doping during MBE is readily achieved but difficult to control. Te tends to accumulate on the

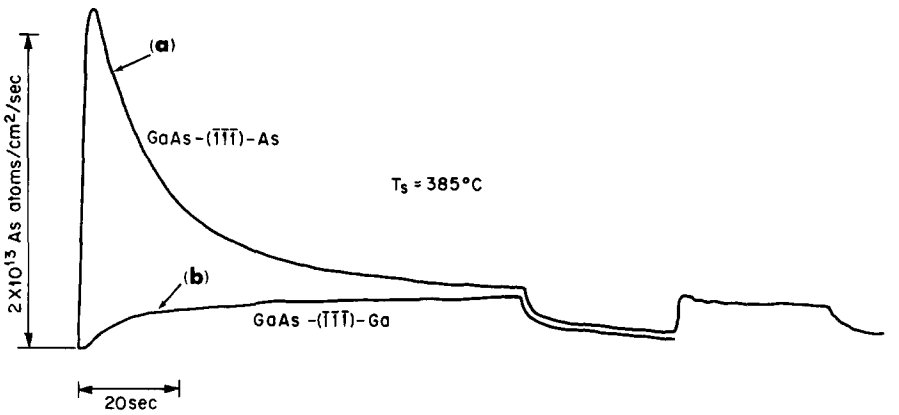

FIG. 14. Time dependence of As_2^+ signal when a Te_2 beam is incident on (a) a $(\bar{1}\bar{1}\bar{1})$ GaAs surface with As-stabilized structure and (b) the same crystal with Ga-stabilized surface structure.

surface so that the doping profile is not uniform, and the film morphology is adversely affected by the Te surface excess. This is apparently a situation in which a stable surface compound (GaTe) is formed. Thus for submonolayer concentrations the sticking coefficient for Te on GaAs is unexpectedly near unity.

(b) $S < 1$

Zn.[36] Zn is not suitable as a dopant for GaAs MBE because of its low adsorption energy, 1.37 eV. Zn desorbs rapidly from GaAs above 175°C, and for a growth temperature of 500°C an incident Zn flux of $\sim 2.6\times10^{20}$ atoms/cm^2 sec (equivalent to 1.6 torr) would be necessary to maintain any appreciable Zn concentration on the surface.

C.[93] Photoluminescence measurements have shown that C is a frequent residual acceptor in MBE GaAs grown from Ga and elemental As. Residual hole concentrations as high as $\sim 1\times10^{16}$ cm^{-3} have been measured in some layers. As an intentional dopant C would not normally be present on the surface in quantities sufficient to affect the surface morphology as discussed earlier; however, it is difficult to find an easily controllable source of C since the sticking coefficients of carbon-containing gases such as CO or C_2H_4 are extremely low on GaAs (though much higher on $Al_xGa_{1-x}As$).

Mg.[35] Mg is at present the most useful p-type dopant for MBE GaAs and $Al_xGa_{1-x}As$. Net acceptor concentrations as high as 10^{19} cm^{-3} have been achieved. The main problem with the use of Mg is the low sticking coefficient which is also a strong function of Al concentration. Figure 15 shows values of the Mg sticking coefficient deduced from the measured carrier concentration as a function of Al concentration in $Al_xGa_{1-x}As$. The data were obtained from six individual MBE layers grown at 560°C with 10^{14} Mg/cm^2 sec, 10^{15} Ga/cm^2 sec and 5×10^{15} As_2/cm^2 sec; only the Al flux was varied. Since the Mg flux was constant, the increase in the hole concentration must be due to an increase in Mg sticking coefficient. Cho and Panish proposed that the increase might be the result of oxygen contamination on $Al_xGa_{1-x}As$, with bonding of Mg to surface oxygen. An alternative explanation is that Mg is more strongly adsorbed on the ternary surface than on GaAs. If we assume that the bulk Mg concentration N_A is proportional to the surface concentration,

$$(N_A)^{2/3} = \beta n_s \tag{12}$$

then since the sticking coefficient $S \ll 1$, the desorption rate Γ is very nearly equal to the incident Mg flux F, and hence the surface lifetime τ is given by

$$\tau = \frac{n_s}{\Gamma} \cong \frac{N_A^{2/3}}{\beta F}.$$

Assuming that the adsorption energy and thus the surface lifetime are functions of the Al concentration x, then from eqn. (7)

$$\ln \tau(x) - \ln \tau(0) = \frac{E_d(x) - E_d(0)}{RT} = \tfrac{2}{3}[\ln N_A(x) - \ln N_A(0)].$$

From the data of Cho and Panish,

$$\ln N_A(0.2) - \ln N_A(0) = 6.2. \tag{15}$$

Then

$$E_d(0.2) - E_d(0) = 0.30\ \text{eV}. \tag{16}$$

This is not a large increase in binding energy, and seems to be explainable in terms of interaction between Al and Mg.

If it is assumed that the proportionality constant $\beta = 1$, i.e. that the concentration of Mg is uniform throughout, then under the conditions used by Cho and Panish for GaAs $n_s = 7\times10^{10}$ Mg/cm^2 and for $Al_{0.2}Ga_{0.8}As$ $n_s = 4.2\times10^{13}$ Mg/cm^2. Since a new surface structure, GaAs(100)–2–Mg, was observed when a Mg beam was incident, the value of 7×10^{10} Mg/cm^2 for GaAs surfaces seems improbably low. Matysik *et al.*[94] studied the interaction of Mg beams with Ge surfaces and observed that reaction to form Mg_2Ge occurred above 250°C. The situation is even more complex with $Al_xGa_{1-x}As$ since stable Mg compounds exist with all three components. Very likely the surface concentration is considerably higher than in the bulk, though this has not been measured. In view of the value of Mg as a p-type dopant, detailed studies of Mg–GaAs surface reactions would seem highly desirable.

It is evident that the incorporation of impurities into MBE GaAs and $Al_xGa_{1-x}As$ is not well understood at present. So far the empirical approach

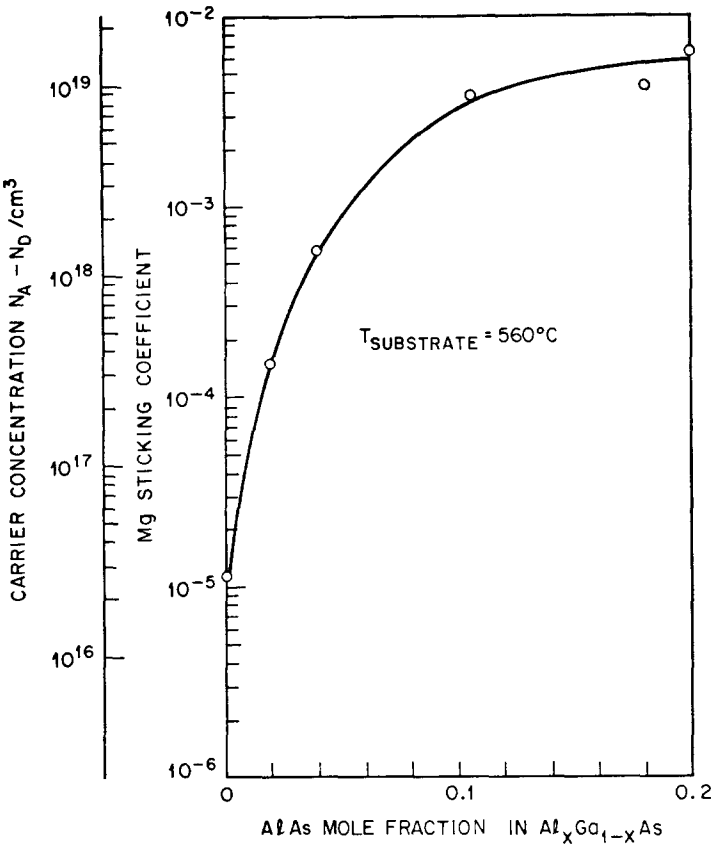

FIG. 15. Measured carrier concentration and calculated sticking coefficient for Mg as a function of Al concentration in $Al_xGa_{1-x}As$. (Ref. 35.)

has yielded *n*- and *p*-type impurities which can be used in device fabrication discussed in Section V, but future device demands may require better control over doping level and uniformity which can be achieved most readily with a detailed understanding of the incorporation mechanisms.

IV. Evaluation of MBE layers

In this section various properties of the epitaxial layers such as surface morphology, electrical and optical characteristics will be discussed. The ability to grow a uniform, epitaxial layer with a large area and featureless surface is of great importance to planar device fabrication technology. The electronic and optical quality of the layers is crucial for high frequency and light-emitting device performance. Advances in the quality of MBE layers depend upon rapid and pertinent evaluations of the layers, and, in particular, non-destructive methods are of special interest. These include phase contrast microscopy, electron diffraction, photoluminescence, reflectivity, and Hall effect measurements.

A. *Surface morphology*

A variety of topographical defects, e.g. pyramids, mounds, dislocation lines, and dendrites, have been observed on the epitaxial layers[1,32,70,91] by examination with a Nomarski interference contrast microscope and electron microscope. Pyramids and mounds are usually caused by residual surface contamination; careful substrate preparation reduces them to a minimum. Dislocation lines are usually caused by either (1) a strained substrate due to stress produced by clamps holding the substrate, or (2) a lattice mismatch between the epitaxial film and the substrate in the case of heteroepitaxy. Dendritic growth usually results from faulty epitaxial conditions, such as growth temperature, deposition rate, and As/Ga ratio in the molecular beam in the case of growing GaAs. Surfaces of layers grown on substrates as large as 2×2 cm, when prepared and grown as described in Section II, have no growth-induced surface features,[91] as demonstrated in Fig. 9c.

Thermally cleaned substrates are usually fairly rough on a microscopic scale. The reduction of this roughness with increasing film thickness is indicated by the RED pattern and electron micrographs in Fig. 9. The smooth surfaces produced by MBE allow very flat, uniform electrical junctions and heteroepitaxial interfaces to be produced. For example, Fig. 1 shows a {110}-cleaved cross-section of alternate layers of GaAs and $Al_xGa_{1-x}As$ when examined with a scanning electron microscope. Each layer is 5000 Å thick. The figure illustrates that reproducible, uniform epitaxial layers can be grown by MBE with precise control of layer thickness.

B. *Hall measurements*

Uniformly doped layers 5 to 10 μm thick were grown on Cr-doped semi-insulating substrates which had resistivities larger than 10^7 Ω cm. Ohmic

contacts were provided by a capacitor discharge bonding technique with a 50-μm diameter Sn-doped Au wire for n-type epitaxial layers and a Zn-doped Au wire for p-type epitaxial layers. The magnetic field used in the measurement was 0.33 Weber/M^2. With the Van der Pauw technique, the carrier concentrations were determined from n or $p = 1/qR_H$, where q is the electron charge and R_H is the Hall coefficient, and the mobilities were determined from $\mu = R_H/\rho$, where ρ is the resistivity.

Figure 16 shows the dependence of the room temperature Hall mobility on the electron and hole concentrations in comparison to the published LPE data and theoretical curve of Rode and Knight.[95] The highest room temperature electron mobility measured for MBE GaAs is $\mu = 7600\,\text{cm}^2/\text{V sec}$ when the layer was doped with Si to a concentration of $N_D - N_A = 1.3 \times 10^{15}/\text{cm}^3$. For a given electron concentration, Sn- and Si-doped layers have higher mobilities than those doped with Ge. This is probably due to the amphoteric nature of Ge[88] which produces some carrier compensation.

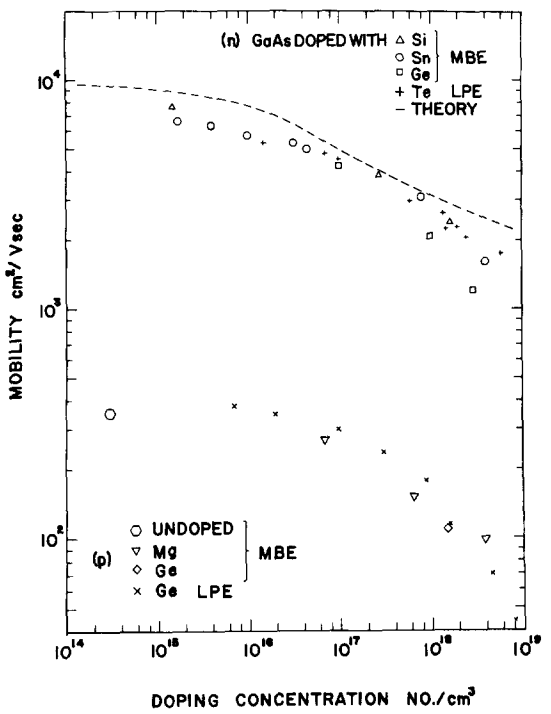

FIG. 16. Room-temperature Hall mobility as a function of doping concentration. Also indicated are results with Te-doped LPE layers (A. R. Goodwin *et al.*, *Proc. Int. Symp. on GaAs, 2nd, Dallas, Texas* (1968)) and Ge-doped LPE layers (F. E. Rosztoczy *et al.*, *J. Appl. Phys.* **41**, 264 (1970)).

When growing GaAs, the As_x beam may be supplied by either heating undoped polycrystalline GaAs[32] or pure As.[59] The former consists mostly of As_2 while the latter consists of As_4. Since the commercially available undoped polycrystalline GaAs contains a large amount of Si impurity ($\sim 10^{16}/\text{cm}^3$), layers grown with this source have the unintentionally doped level of $N_D - N_A \approx 5 \times 10^{15}/\text{cm}^3$. While the layers grown by evaporating polycrystalline GaAs exhibit n-type conductivity, the layers grown by evaporating pure Ga and pure As exhibit p-type conductivity.[48] The background carrier concentration is also reduced to $N_A - N_D \approx 2 \times 10^{14}/\text{cm}^3$, and with $\mu = 360\,\text{cm}^2/\text{V sec}$ at room temperature. Both the n-type and the p-type MBE layers have mobilities comparable to those grown by the LPE method.

The temperature dependence of the Hall mobilities for several representative samples is shown in Fig. 17. Curves (a–c) are of n-type samples and curves (d–e) are of p-type samples. The

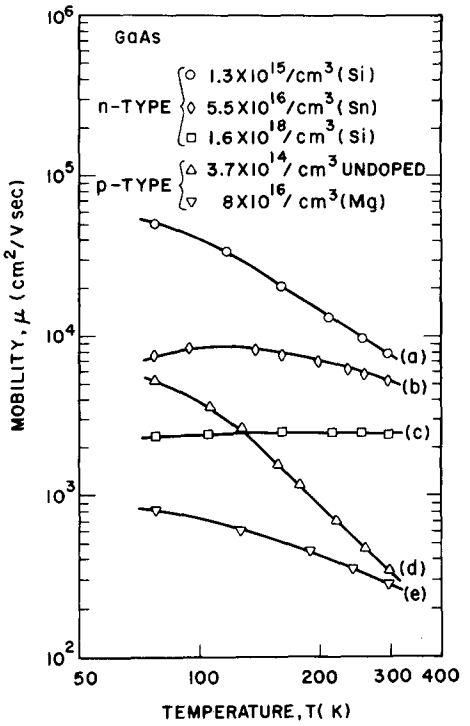

FIG. 17. Hall mobilities as a function of temperature for p- and n-type GaAs MBE layers.

mobility in pure (intrinsic) sample is governed by three scattering mechanisms:[95] (1) dominated by polar-mode scattering above 100 K, (2) piezoelectric and acoustic-mode scattering between 60–80 K, and (3) ionized-impurity scattering below 60 K. Curves (a) and (d) of Fig. 17 are of two quite pure samples, $N_D - N_A = 1.3 \times 10^{15}/\text{cm}^3$ and $N_A - N_D = 3.7 \times 10^{14}/\text{cm}^3$ respectively. These two curves illustrate the variation of mobility as a function of temperature where the above-mentioned scattering mechanisms dominate different temperature regions. When the samples are doped with impurity concentrations higher than $10^{16}/\text{cm}^3$, the impurity scattering mechanism dominates even at higher temperature; the variation of mobility as a function of temperature becomes less pronounced as illustrated in curves b, c, and e.

C. *Photoluminescence*

Photoluminescence is the production of radiative emission from a material by photon excitation. The photon energy must be higher than the bandgap of the semiconductor in order to generate carriers in the valence and conduction band. It is the process of the recombination of these carriers (electrons

and holes) that characterize the semiconductor material.

Photoluminescence has been used to study radiative band-to-band recombination and radiative transitions through impurity centers.[96-99] The spectral shape and peak position may also be used to estimate the impurity concentration and degree of compensation.[100] The luminescent intensity for a given impurity level and excitation level reveals the quality of the crystal because defects such as dislocations will reduce the luminescence efficiency.[101, 102]

Photoluminescence measurements have been made on MBE samples at 300 K and 80 K with an argon laser of approximately 10–30 mW power. The detection system consisted of a Perkin–Elmer prism spectrometer with an Amprex S-1 photomultiplier. Figure 18 shows the room temperature photoluminescence of Sn-doped GaAs layers[68] with doping concentrations varying from $2.5 \times 10^{17}/cm^3$ to $1.2 \times 10^{19}/cm^3$ as determined by Hall measurements. The maxima of these spectra shift toward higher energy and the half-widths broaden when the number of free carriers increases due to the participation of electron states higher into the conduction band. The increase in the relative luminescent intensity as a function of carrier concentration is simply because there are more recombination centers available. The decrease in intensity when the carrier concentration increases beyond $2 \times 10^{18}/cm^3$ is probably due to an increase in nonradiative centers caused by increasing impurity precipitation and vacancy formation at such high doping levels. Despite the slight

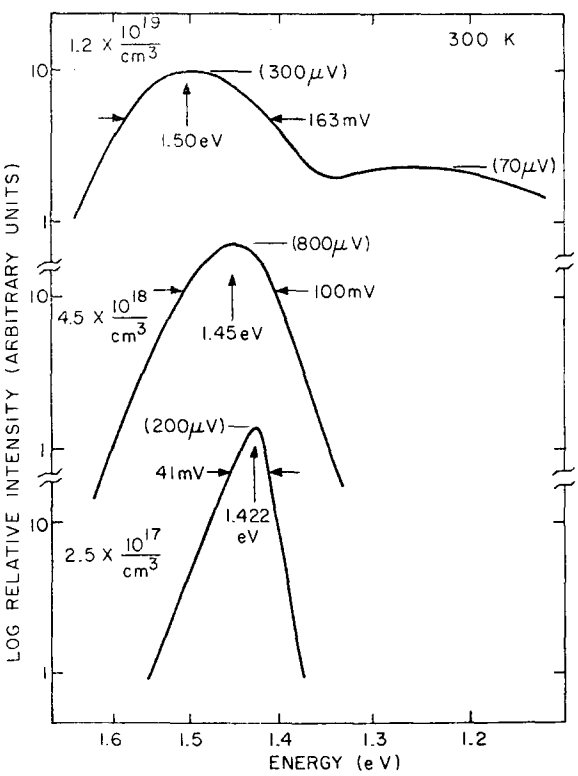

FIG. 18. 300 K photoluminescence spectra of Sn-doped GaAs layers with different doping concentrations. The voltage readings in parenthesis are the relative magnitude of output from the photomultiplier which correspond to the relative photoluminescent intensities.

decrease in luminescent efficiency at $N_D - N_A = 1.2 \times 10^{19}/cm^3$ when GaAs was doped with Sn, the layer grown by MBE still has near-gap radiation higher than the deep-level emission, which makes it superior to most of the commercially available crystals.

While the Si-doped GaAs layers[90] give photoluminescence similar to that of Sn-doped GaAs-layers,[68] Ge-doped layers are quite different.[88] As mentioned earlier, GaAs layers doped *n*-type with Ge are achieved by evaporating Ge onto the substrate while growing GaAs with an As-stabilized surface structure and *p*-type while growing with a Ga-stabilized surface structure. A comparison of the 80 K photoluminescence spectra of these layers both doped to $8 \times 10^{17}/cm^3$ is shown in Fig. 19. The layer in Fig. 19(a) was grown with an As-stabilized surface structure (*n*-type) and has a relatively higher band-to-band transition peak while that in Fig. 19(b) was grown with a Ga-stabilized surface structure (*p*-type), and has a higher band-to-acceptor transition peak. The solid curve and the dotted curve are spectra from focused and defocused laser excitation beams which merely represent results from two different excitation densities. The shift of the photo-luminescence peaks toward higher energy with increasing excitation density is due to a band-filling effect[103] and is a characteristic of compensated crystals.

Since the demonstration of injection lasers prepared by MBE,[104] the need for a high luminescent efficiency layer has prompted extensive re-evaluation of GaAs layers doped with various dopants and grown at different temperatures. It has now been found that Si and Sn doped GaAs layers grown at 620°C have photoluminescence efficiencies comparable to those of layers grown by LPE.[105]

D. *Reflectance*

Photoreflectance is complementary to photoluminescence and is also used to study the band structures of semiconductors. These optical measurements furnish important information for the understanding of solids. However, the surface preparation of the sample plays an important role in the interpretation of the optical data because of the small penetration depth of the incident light. For instance, for a mechanically polished surface the reflectance may take place entirely within the distorted surface layer. Epitaxial films are attractive in that they do not have this distorted surface layer which is always present in a polished bulk crystal. In this section, we will only consider the use of reflectance as a measure to compare the quality of the "as-grown" surfaces of MBE and LPE layers.

Reflectance spectra have been used to evaluate microstrain and surface damage in semiconductors.[106, 107] Local strains in general provide scattering centers for the electrons and thus tend to broaden the optical structure as illustrated earlier by Sell and MacRae.[107] In the study of reflectance, the near edge transition is very weak or not detectable when the doping level is higher than $10^{17}/cm^3$. However, for GaAs the transitions of the spin–orbit split valence band to the non-degenerate conduction band along the [111] direction in *k*-space (E_1, $E_1 + \Delta_1$)[108] are not

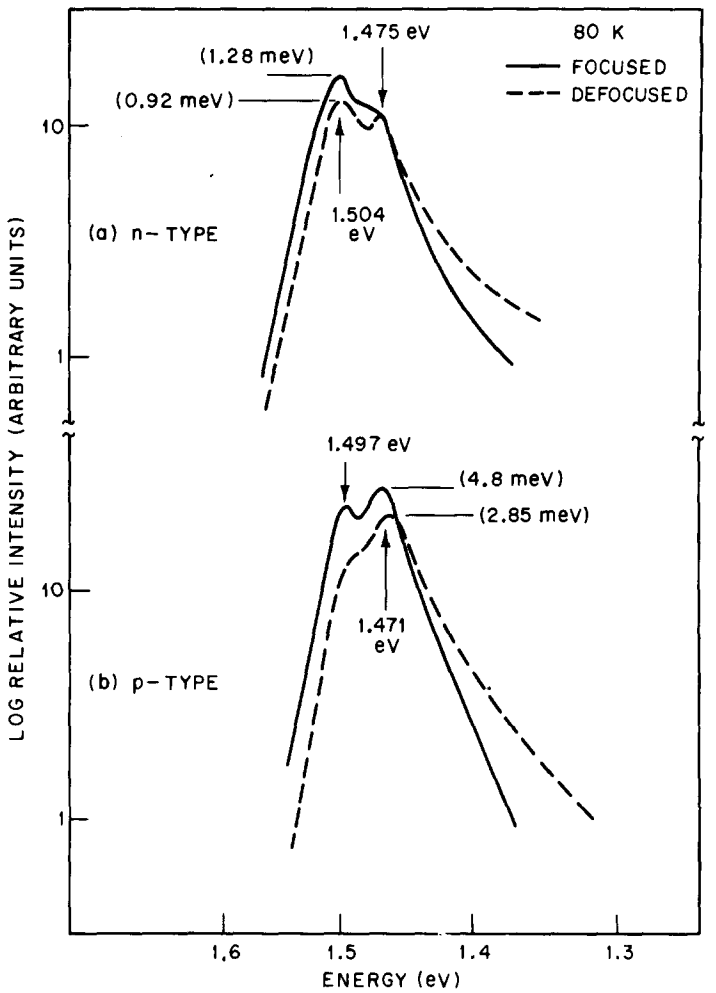

FIG. 19. A comparison of 80 K photoluminescence spectra under the same laser excitation (a) Ge-doped GaAs grown with an As-stabilized surface structure formed an *n*-type layer. (b) Ge-doped GaAs grown with a Ga-stabilized surface structure formed a *p*-type layer. Both of these layers have $|N_d - N_a| \approx 8 \times 10^{17}/\text{cm}^3$. Solid line, focused; dotted line, defocused.

sensitive to the doping levels. Therefore, the sharpness of these two peaks is used for the comparison of surface qualities. The slope or sharpness of the spectra is best represented by the value of its derivative. For the convenience of calibration, from sample to sample, they are compared with the value $(dR/dE)/R$ where the derivative with respect to energy is normalized with the total reflectance, R. The reflectance measurements are performed in a double-beam scanning spectrometer described by Sell[109] where a monochromatic light beam is alternately focused onto the sample and a reference. The resulting signals are processed electronically through a mini-computer and the value $(dR/dE)/R$ is plotted automatically.

Figure 20 shows the values of $(dR/dE)/R$ of the E_1 and $E_1 + \Delta_1$ transitions of *n*- and *p*-type epitaxial GaAs layers grown by MBE and LPE techniques.[110] It is seen here that the transitions are sharper for the samples grown by MBE, thus illustrating that the surface quality of MBE layers is superior to that of LPE layers in terms of local strain. This may be the result of the lower growth temperature used in MBE.

E. *Schottky barriers and p–n junction*

The rectifying metal-semiconductor contact, Schottky barrier, can be used as a tool to analyze fundamental physical parameters, doping profiles, and the reverse breakdown voltage of the epitaxial layer. The reverse breakdown voltage is a measure of the perfection of the crystal because any defects will lead to excess current and result in a premature breakdown. Schottky barriers are used in a variety of microwave devices such as clamped transistors, field-effect transistors, varactors, frequency converters, and IMPATT diodes.

The current–voltage characteristics for an Au Schottky barrier on a GaAs layer with $N_D - N_A = 5 \times 10^{15}/\text{cm}^3$ is shown in Fig. 21.[91] The area of the diode is about 8×10^{-5} cm^2. No leakage current was detected down to 10^{-11} A, and the current–voltage varied as $\exp(qV/nkT)$, with $n = 1.08$. The value n is usually referred to as a quality factor, and $n = 1.08$ is considered to be near ideal condition. The reverse breakdown voltage of 105 V as shown in Fig. 21 is equal to the breakdown voltage expected for a bulk crystal.[111]

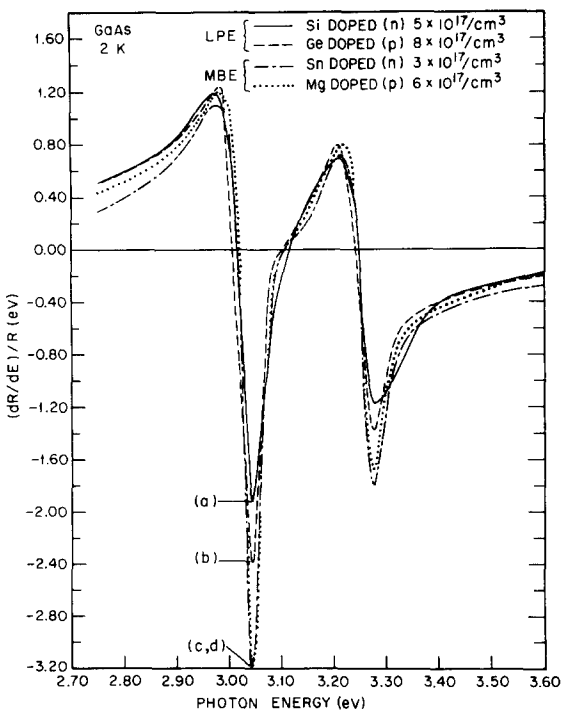

FIG. 20. Derivative of the 2 K photoreflectance $(dR/dE)/R$ of layers grown by LPE (a, b) and MBE (c, d). (Courtesy of S. E. Stokowski.)

Impurity incorporation during MBE can also be controlled to give very uniform doping profiles. Figure 22 shows the net donor concentration as a function of distance into the film for two typical GaAs samples doped with Ge. The doping profiles were measured by the differential capacitance[112] of Schottky barrier diodes made from the films. For a sample 1×1 cm, 70% of the diodes gave carrier concentrations within 5% of the average value, indicating lateral uniformity as well as the uniform profile indicated by the figure.

Many semiconductor devices require p–n junctions which should ideally be characterized by low reverse leakage currents and sharp breakdown voltages. The properties of GaAs p–n junctions when the incorporation of known impurities into the layer was by the co-deposition of pure Ga and As and dopants from separate effusion sources have been reported.[88,91] The preparation of such structures usually involves the growth of a 2 μm thick n^+ buffer layer on an n-type substrate. An active n-type layer typically doped with Sn or Si to $5 \times 10^{17}/\text{cm}^3$ and a p-type layer doped with Mg to $5 \times 10^{16}/\text{cm}^3$ were subsequently grown on the n^+ buffer layer. The I–V characteristics of a mesa diode fabricated on such a structure is shown in Fig. 23.[91] The forward current varies as $I = I_0 \exp(qV/nkT)$ where $n = 1.8$. No leakage current was detected in either the forward or the reverse biased conditions.

V. Device applications of MBE

In previous sections it has been suggested that the most significant feature of MBE for device preparation is the control over thickness, composition and impurity level which can be obtained. While MBE is not as rapid as conventional epitaxial techniques, there are a number of devices where growth control is crucial to the device operation.

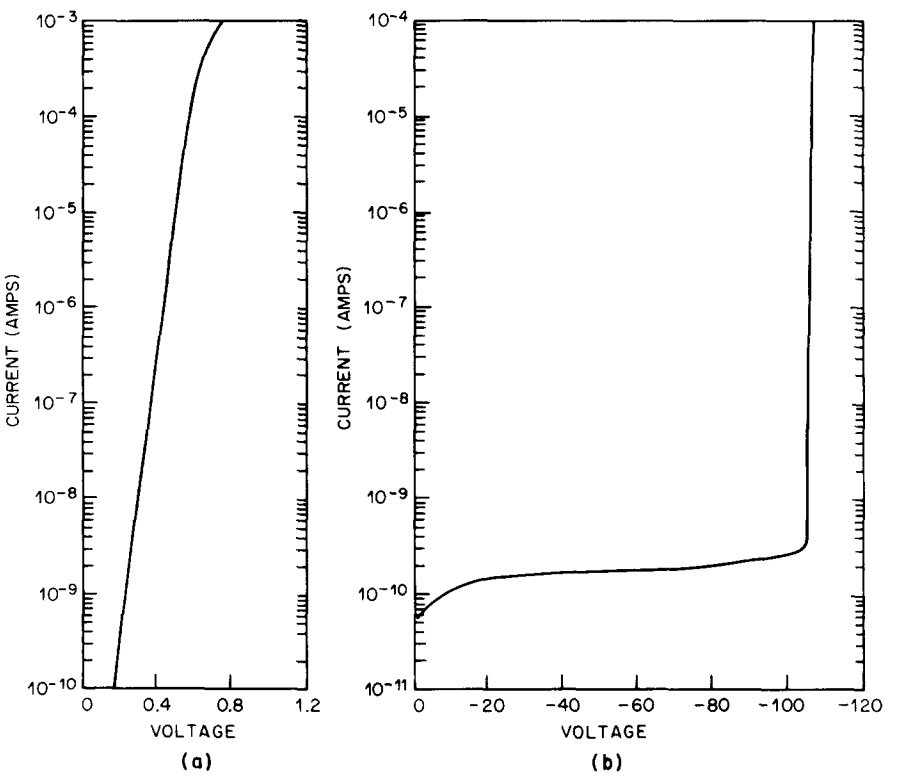

FIG. 21. Current–voltage characteristic for Au Schottky barrier on an MBE layer with $N_d - N_a = 5 \times 10^{15}/\text{cm}^3$: (a) forward bias; (b) reverse bias. The diode area is 8×10^{-5} cm^2. (Ref. 91.)

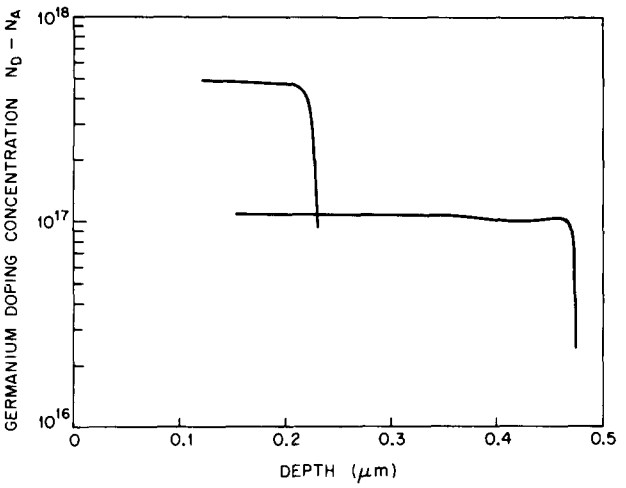

FIG. 22. Doping concentration as a function of film depth of two typical samples showing the ability to prepare uniform doping profiles.

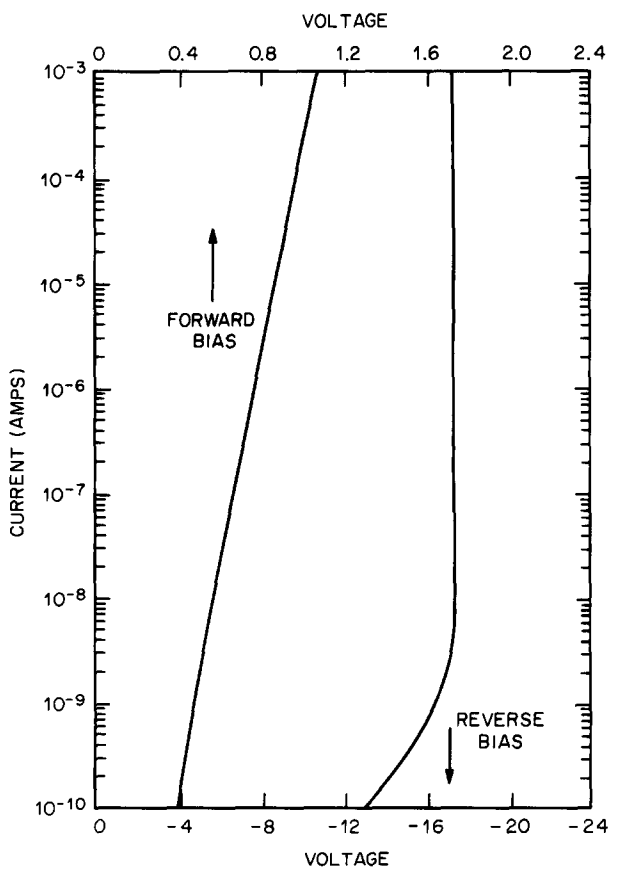

FIG. 23. Current-voltage characteristics of an MBE GaAs p–n junction. The area of the diode is 8×10^{-5} cm^2.

Two general types of devices for which this is true are those intended for microwave operation, including IMPATT (impact avalanche and transit time) diodes, varactors, and mixer diodes, and those designed for optoelectronic functions such as injection lasers. Many of these have now been successfully grown by MBE and their performance will be described in this section.

A. *Varactor*

A hyperabrupt varactor is a diode with a doping profile tailored such that a small change in reverse bias results in a large change in diode capacitance due to the widening of the depletion layer. A hyperabrupt varactor has a doping profile of N_D–$N_A = BX^m$, where N_D is the donor concentra-

tion and N_A is the acceptor concentration, X is the distance from the surface of the epitaxial layer, B is a constant and m is <0. $m<0$ implies that the doping profile decreases as a function of distance away from the junction (in the case of a Schottky barrier diode, the concentration decreases with depth into the crystal) following some power law characterized by the value m. The differential capacitance is $C \propto (\varphi - V)^{-n}$, where $n = 1/(m+2)$, φ is the effective barrier height, and V is the bias voltage.[111] For a particular application in tuning circuits, it is desirable to have the resonant frequency of the circuit proportional to the bias voltage. This can be accomplished by a wafer with a doping profile $N_D - N_A = BX^{-3/2}$ and therefore $(\varphi - V) \propto C^{-1/2}$.

A doping profie of a hyperabrupt Schottky barrier varactor giving the $(\varphi - V) \propto C^{-1/2}$ relationship is shown in Fig. 24.[48] This device was made from a Sn-doped GaAs layer grown while varying the Sn deposition rate in a predetermined manner. Figure 25 shows capacitance as a function of bias voltage for other MBE devices grown with different doping profiles to obtain a range of values of n.[48] It is noteworthy that MBE can produce an abrupt change in carrier concentration that results in a capacitance–voltage relationship of $n = 4$; a small bias change of less than 1 volt results in a change in capacitance of a factor of 10.

B. *IMPATT diode*

The avalanche transit time diode[113] is a solid-state device capable of generating microwave power with very high efficiency. The diode is reverse biased by a current source which causes the voltage across the junction to increase until avalanche breakdown occurs. The avalanche breakdown generates a large number of carriers which drift down a low doped region until they are finally collected at an n^+ terminal. The voltage across the junction then increases, again generating another group of avalanche carriers. The frequency of this relaxation oscillator is determined by the length of the drift region and the saturation velocity of the carriers.

The IMPATT diode was first proposed by Read;[113] a modified version[114–116] which has a substantially higher DC to RF conversion efficiency compared to conventional flat doping profile IMPATTs is referred to as a low–high–low profile IMPATT to indicate the doping composition of the active layers. The doping profile of an example of this structure grown by MBE[117] is shown in Fig. 26. A narrow avalanche zone is confined between the metal Schottky barrier (p^+ contact) and an extremely thin, highly doped n^+-layer. A moderately doped n-type drift region and an n^+ buffer layer and contact complete the structure. The structure clearly represents a severe test of doping control.

Low–high–low IMPATTs have been grown by MBE with very promising characteristics.[117] For example, the distribution of the reverse breakdown voltages of thirty-one randomly selected units fabricated from a single MBE wafer are plotted on a probability coordinate shown in Fig. 27. The reverse breakdown voltage was determined at 1 mA and the area of each diode was 2×10^{-4} cm^2. A standard deviation is defined as the range of ordinate values for those units lying between 16% and 50%. The breakdown voltage distribution is very uniform with the standard deviation being only 1 volt. The median value is 45.3 volts.

The RF evaluations of the diodes were carried out in a coaxial reflection-type amplifier using a locked-oscillator technique for measuring the FM noise.[118] Figure 28 shows noise-power and efficiency characteristics of MBE IMPATT diodes. The operating frequency is 11.7 GHz for diodes having the doping profile shown in Fig. 26. The diode output power normalized to 1 mW is plotted in dbm units where 30 dbm corresponds to 1 W output, and 34.77 dbm corresponds to 3 W output. It is seen here that for 3 W output, the efficiency is 18% and the noise measure only 44 db. The solid line in Fig. 28 is calculated from large-signal performance modeling[119] and is in agreement with the experimental values.

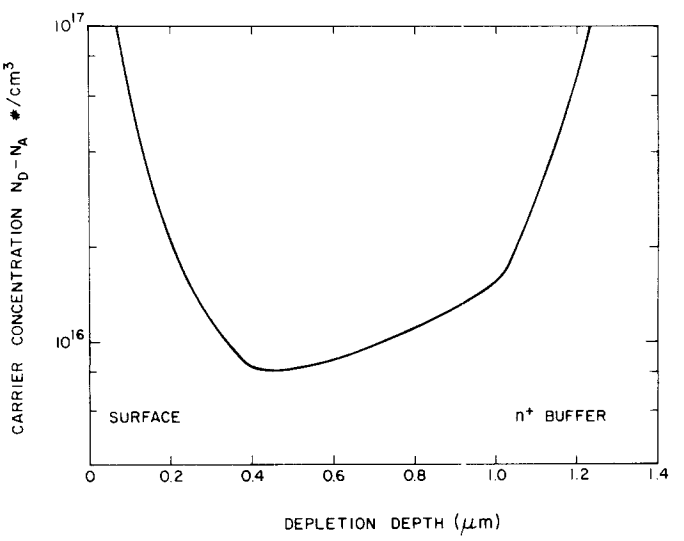

FIG. 24. Doping profile of a hyperabrupt Schottky barrier varactor giving the $C^{-1/2} \propto (\varphi - V)$ relationship for $0.3 \geq V \geq -1.7$ V.

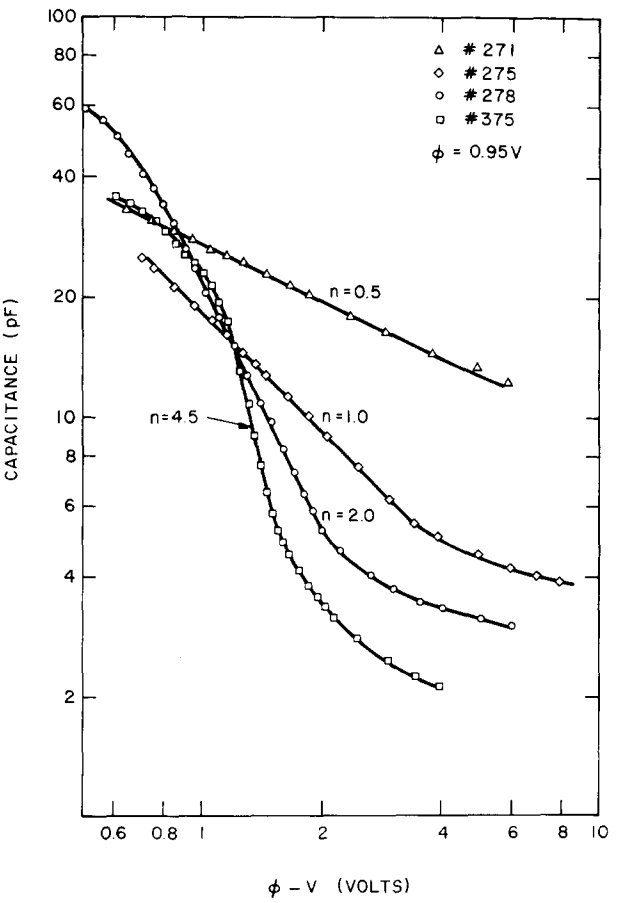

FIG. 25. Capacitance variation as a function of biasing voltage for MBE layers with different doping profiles. (Ref. 48.)

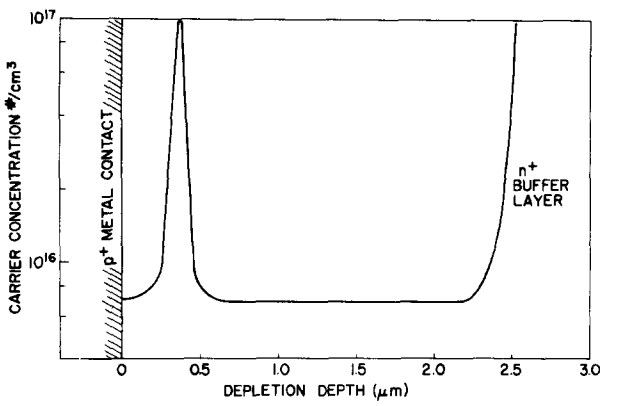

FIG. 26. Typical carrier profile of a low–high–low IMPATT diode.

The efficiency and power capabilities of these diodes are higher than those usually obtained with flat doping-profile diodes but without an increase in noise measure. The performance so far makes them quite attractive for microwave power amplification applications.

C. *Mixer diode*

As the name implies, this microwave diode can mix two microwave signals to generate sum and difference frequencies, thus converting the information-bearing signal up or down in frequency. The conversion is accomplished by beating the input signal with the signal of a local oscillator in the mixer, where the local oscillator is simply a continuous-wave oscillator operating at a frequency slightly different than the signal-bearing frequency. The purpose of the frequency conversion is to make it easier to process a signal for amplification, detection, switching, modulation, and filtering at a lower frequency where conventional lumped circuits can be used.

The basic structure of a GaAs Schottky barrier mixer diode consists of an *n*-type active layer with

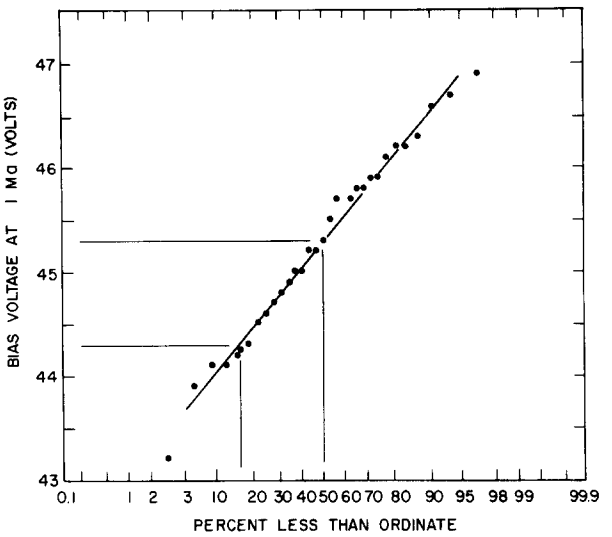

FIG. 27. Distribution of breakdown voltages of randomly selected low–high–low IMPATT diodes fabricated from the same wafer. Figure shows that a standard of deviation is only one volt. (Courtesy of C. N. Dunn and R. L. Kuvas.)

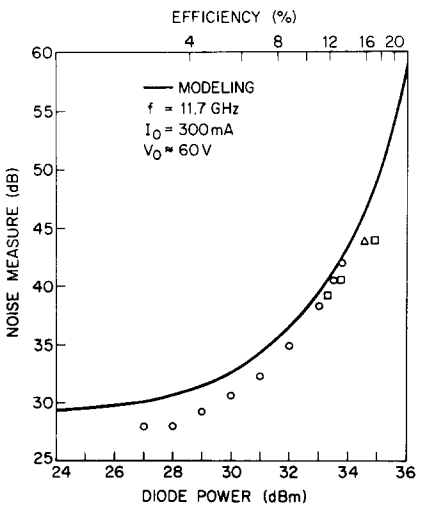

FIG. 28. Noise-power and efficiency characteristics of MBE IMPATT diodes. The solid line is the calculated value from large-signal performance modeling. (Ref. 117.)

a carrier concentration in the low $10^{17}/cm^3$ range and a thickness of 2000 to 3000 angstroms. This active layer is grown on an n^+ buffer layer with a carrier concentration $\sim 2 \times 10^{18}/cm^3$. An ohmic contact is formed on the n^+ buffer layer while the metallic Schottky barrier is formed on the active layer. Since the cut-off frequency is inversely proportional to the capacitance of the device, the area of the Schottky barrier is usually very small, of the order of 10^{-7} cm^2, in order to reduce the capacitance. However, in many cases the parasitic capacitance resulting from the leads and encapsulation limits the cut-off frequency. Diodes now being developed for use in stripline circuitry require gold-beam leads for circuit connections. The parasitic capacitance arising from the beam anchor area and "interconnects" with the n^+ substrate presented a serious problem. A new technology forming planar, electrically isolated GaAs devices has been developed[120] to make the mixer diode compatible with beam-lead technology. This MBE planar technology will be discussed in more detail in Section VI.

Mixer diodes fabricated on the MBE planar electrically isolated areas showed low parasitic capacitance. A typical value of the capacitance is in the order of 0.02 pF. The conversion loss which is the ratio of available power at the signal frequency to the available power at the difference frequency (intermediate frequency) is a measure of the quality of the mixer diode. When the MBE mixer diodes were tested in double-balanced down converter configuration, the conversion loss was 5.3 dB at 51.5 GHz.[121] The measured conversion loss as a function of frequency and the calculated values[122] are plotted in Fig. 29. The minimum of the curve represents the loss due to the diode while the increase in conversion loss at different frequencies

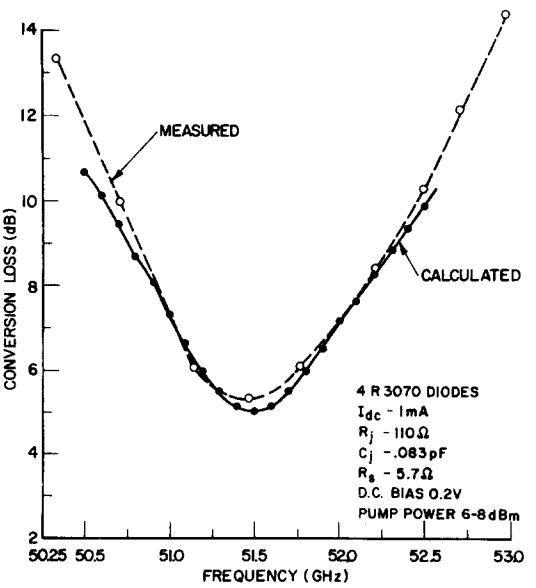

FIG. 29. Measured and computed conversion loss for balanced mixer diodes. (Ref. 121.)

from the minimum point is due to the loss from the tuning circuit used in the measurement. This demonstrates that mixer diodes grown by MBE planar technology can use beam-lead technology and yet have low parasitic capacitance and low conversion loss.

D. *Schottky barrier field effect transistor (FET)*

The Schottky-barrier FET has a structure similar to that of a junction FET in which the diffused junction gate is replaced by a metal–semiconductor barrier gate. There is a considerable interest in the GaAs FET as a low-level, low-noise amplifier at microwave frequencies. The material specifications vary widely for this device, but the basic structure requires a thin *n*-type epitaxial layer on a semi-insulating substrate. A typical example for such a structure designed for operation at 4 GHz is a layer with carrier concentration in the mid-$10^{16}/cm^3$ range and 5000 Å thick. The device performance requires precise control in layer thickness and uniformity; a thickness variation of a factor of 2 will result in an order of magnitude change in the d.c. parameters of the device. In order to assure very uniform deposition over a large area substrate, the substrate must be positioned far (e.g. 20 cm) from the source so that the angular variation in beam intensity ($\sim \cos\theta$) is minimal across the substrate. The penalty for placing the sample far from the source is a reduction in the growth rate. However, the FET structure requires only less than a micron deposition; a slow growth rate may be advantageous from the point of view of precise control in layer thickness.

The current–voltage (I_{DS}–V_{DS}) characteristics of an FET made on an MBE GaAs layer are shown in Fig. 30.[123] The RF measurements on these devices have not been completed. However, a significant feature illustrated here is that MBE can produce a GaAs Schottky barrier FET with I–V characteristics that do not exhibit the hysteresis which is often found with those grown by other techniques.[124–125] It has been suggested that hysteresis is due to filling and emptying of traps at the substrate–epitaxial layer interface.[124]

It is important to note that the devices described previously in this section do not need to have the active layer grown on the substrate surface directly; a highly conducting buffer layer is first grown, providing a more perfect starting surface for the actual device. Because of the necessity for a semi-insulating layer under the active layer for the FET, it is more convenient to grow the active layer directly on the available semi-insulating substrate. This makes the preparation of the substrate an important factor for the quality of the epitaxial layer. The traps at the substrate–epitaxial layer interface could be due to the improper preparation of the substrate surface. The MBE layers used in the FET fabrication were grown on substrates which were first cleaned *in situ* by argon ion sputtering to assure atomically clean surfaces for the epitaxy. This may be the reason for the absence of hysteresis in the I–V characteristics of MBE-grown FETs.

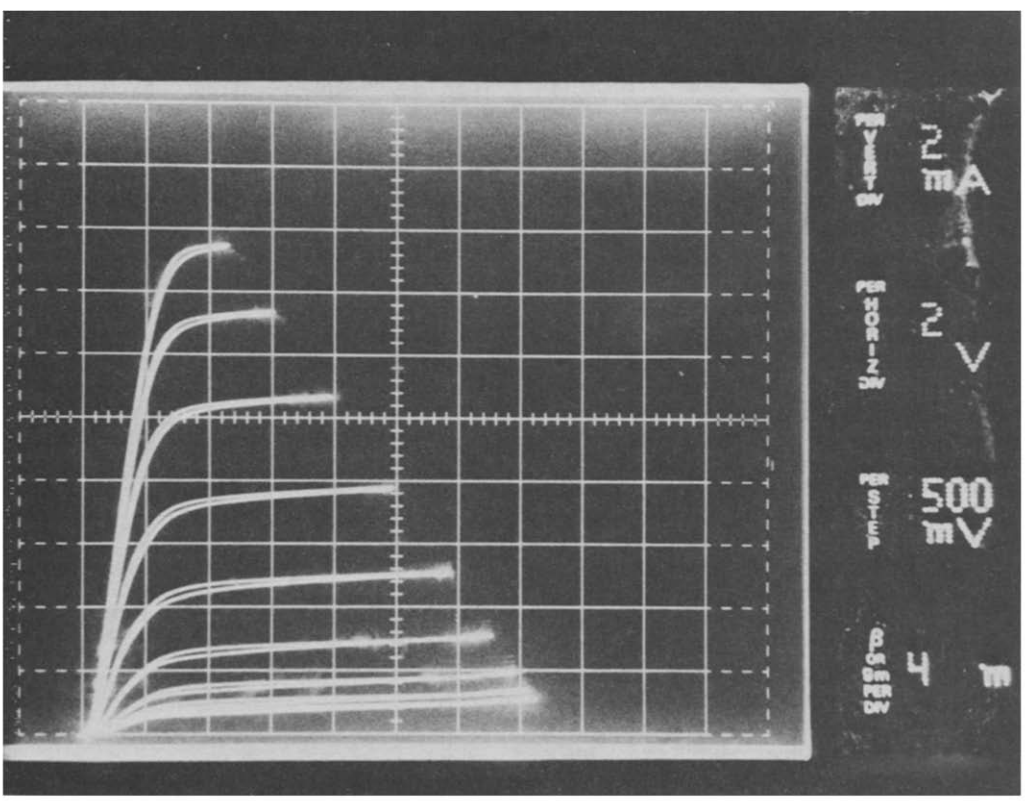

FIG. 30. Drain to source current–voltage characteristics of an MBE field effect transistor. (Courtesy of R. B. Fair.)

E. *Injection lasers*

The potential importance of the room-temperature CW injection laser to optical communications systems has stimulated a great effort to understand and improve its efficiency ever since it was first demonstrated in a structure grown by liquid phase epitaxy.[126,127] The basic structure of a double heterostructure (DH) laser consists of a thin GaAs active layer sandwiched between two $Al_xGa_{1-x}As$ layers with $X \approx 0.3$. The reason for such a composition is that GaAs has a lower energy gap and a higher index of refraction than $Al_xGa_{1-x}As$; the structure results in both carrier and optical confinement in the active layer.[128] When grown on an *n*-type GaAs substrate, the first $Al_xGa_{1-x}As$ layer is *n*-type, the active GaAs layer may be either *n*- or *p*-type, and the second $Al_xGa_{1-x}As$ layer is *p*-type; a heterojunction is thus formed. When the junction is forward biased minority carrier injection into the active region creates a high density of both electrons and holes whose recombination leads to light emission at a wavelength characteristic of the material. If the absorption of the spontaneously emitted photons is low enough so that each photon can stimulate further emission before being absorbed, lasing will occur. The absorption of radiant energy due to losses through bulk absorption, scattering, diffraction, and the absorption due to free carriers must be supplied externally from the biasing supply during lasing. The minimum biasing current required to sustain lasing is called the threshold current.

Until recently, liquid phase epitaxy was the only technique capable of controlled growth of GaAs and $Al_xGa_{1-x}As$ layers of sufficient electrical and optical quality for low threshold current lasers. Typically LPE DH lasers which can be operated CW at room temperature have a threshold current less than 2 kA/cm^2 and an active layer thickness less than 0.5 μm. There is some incentive for reducing the active layer thickness since this will produce higher optical and minority carrier densities; however, LPE becomes increasingly difficult to control reproducibly for thinner layers. Since growth control is the main feature of MBE, some considerable effort has been directed toward fabrication of DH lasers from MBE material.

While $Al_xGa_{1-x}As$ layers are readily grown by MBE[1,129] with the addition of an Al source, in early work these films showed low photoluminescent efficiency, implying that non-radiative recombination centers were present. At the same time it was observed by Auger spectroscopy that the sticking coefficient of CO was much higher on $Al_xGa_{1-x}As$ than on GaAs, which suggested that CO contamination might be limiting photoluminescence. With improved vacuum conditions (principally by extensive use of reactive metal film gettering), the CO background was reduced to a barely detectable level during growth, while at the same time the photoluminescent efficiency of MBE $Al_xGa_{1-x}As$ considerably increased. Since the active region in a DH laser is composed of GaAs, the presence of non-radiative centers in the $Al_xGa_{1-x}As$ might not appear serious; however if these centers appear at the interface they will greatly influence the lasing characteristics.

With the improved $Al_xGa_{1-x}As$ layers, MBE lasers have been obtained.[104] Figure 3 shows the growth system used for their preparation. Three groups of effusion cells are used, with each group having an individual mechanical shutter. A schematic representation of the temperature–time schedule for each effusion cell for the growth of a DH laser is shown in Fig. 31(a). The dotted lines indicate the temperature of the cells behind the shutter while the solid lines indicate the temperature of the cells when the shutter is opened. The substrate is heated to 625°C during deposition and the resulting layer thickness and composition are illustrated in Fig. 31(b).

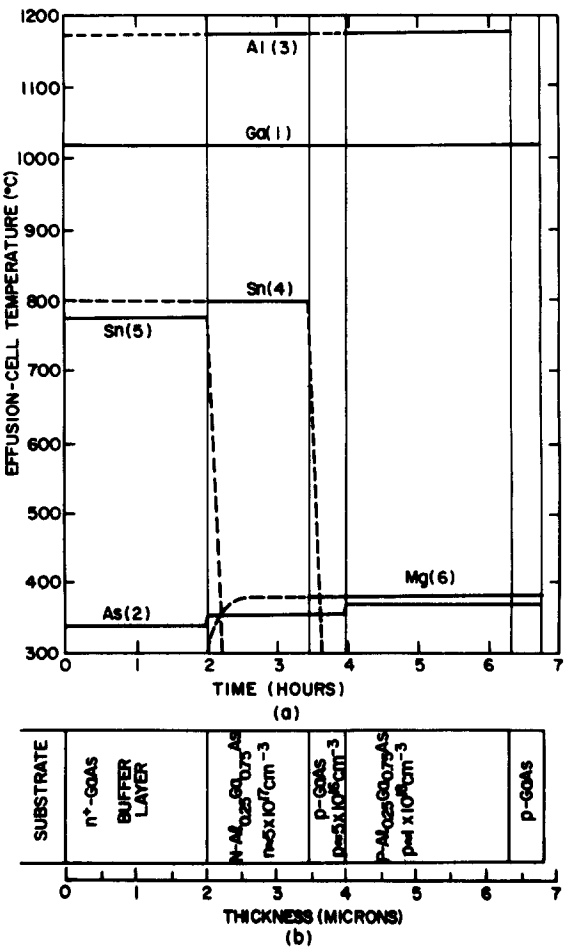

FIG. 31. (a) Temperature–time cycles used to grow MBE five-layer DH lasers. Solid lines indicate shutter was opened while dotted lines indicate shutter was closed. Substrate temperature was 625°C. (b) Schematic representation of the layers grown by the temperature–time cycles in (a). (Ref. 104.)

The cleavage plane of GaAs is {110}. When the epitaxial layer is grown on the {100} substrate there are two mutually perpendicular cleavage planes available normal to the {100} surface. One may use the cleaved surfaces as mirrors to form a Fabry–Perot cavity. A scanning electron micrograph of a cleaved plane showing the cross-section of a MBE DH laser is illustrated in Fig. 32. Preliminary studies showed that this device lased with a threshold current density of 35 kA/cm^2 at room

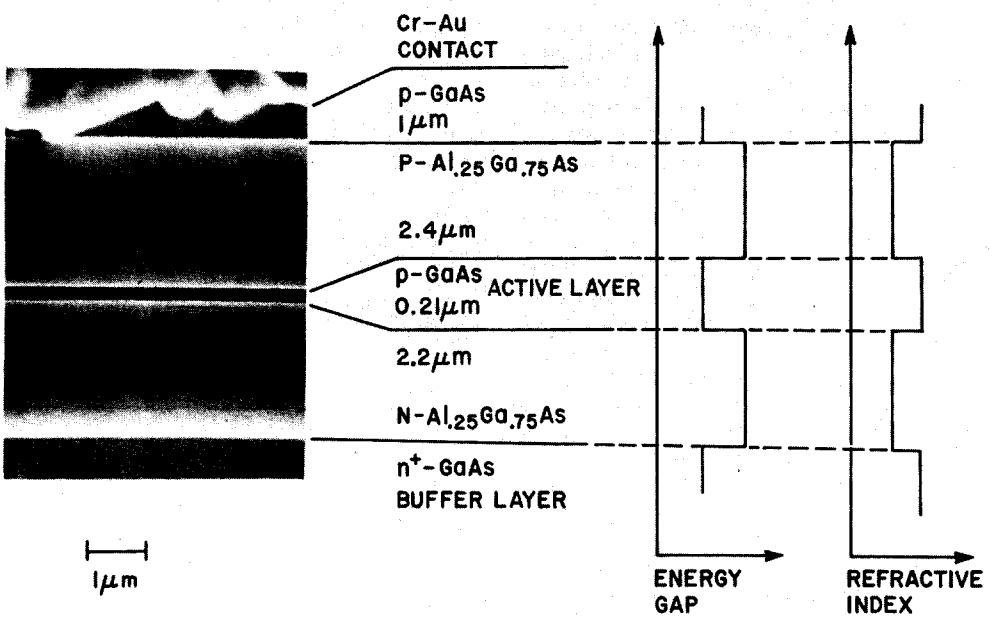

FIG. 32. Scanning electron micrograph of a {110}-cleaved cross section of a DH laser grown by MBE. The step change in energy gap and refractive index for the layer structure is shown to the right.

temperature.[104] The active layer was doped with Mg with a thickness of 0.53 μm, and the cavity length was 350 μm. Annealing the structure at either As-rich or Ga-rich conditions at 750°C for 2 hr reduced the threshold current density to 4 kA/cm^2, while the differential quantum efficiency was 39%. Figure 33 shows the improvement of the lasing characteristics of a MBE DH laser with a Mg-doped active layer before and after annealing. Also indicated in this figure are the characteristics of a LPE DH laser having nearly equal cavity length and cross-sectional area of 5.4×10^{-4} cm^2. It is evident that annealing dramatically improved the quantum efficiency of the Mg-doped MBE laser to

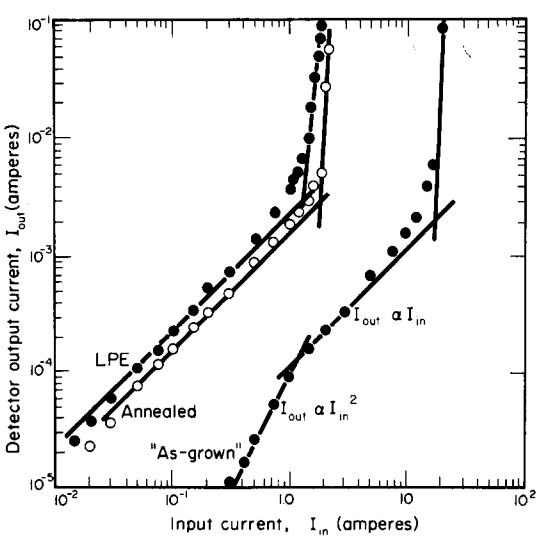

FIG. 33. Detector output current as a function of the input current. The output current is for emission from both mirrors and the external efficiency is taken as I_{out}/I_{in}. Emission from the sawed sides has been ignored. (Ref. 104.)

where the performance approaches that of a LPE laser.

A Mg-doped GaAs film grown by MBE also showed an increase in photoluminescence efficiency by over an order of magnitude after the sample was annealed. This implies that the reduced threshold current of the MBE laser after annealing results from changes in the bulk properties of the Mg doped active layer. It is speculated that non-radiative centers may have resulted from a Mg–O complex due to the highly reactive nature of Mg. Other *n*-type GaAs layers doped with Sn, Si and Ge have shown photoluminescence efficiencies as high as those grown by LPE with no increase in efficiency after annealing. Since the active layer in the DH laser can be either *p*- or *n*-type, MBE lasers are now prepared with *n*-type active layers. The threshold current for lasing at room temperature has improved to 4 kA/cm^2 *without* annealing. In an annealed structure the lowest threshold so far obtained is 2.5 kA/cm^2 and further improvement is expected as the choice of dopant, the doping level, and active layer thickness are optimized.

F. *Optical waveguides*

Progress in injection laser development has also spurred interest in optical waveguides for low loss transmission of light. A waveguide has a central core of refractive index n_1 surrounded by a medium of refractive index n_2, where $n_1 > n_2$. The number of modes which can be guided in such a structure is governed by the dimensions of the guide and the difference in the indices of refraction between the guided region and the medium surrounding it. Epitaxial layers of GaP on CaF_2[33,34] may be used for optical guiding because the index of refraction for GaP is 3.26 and that for CaF_2 is 1.43. One of the most studied systems is GaAs/$Al_xGa_{1-x}As$ because of the success of the DH laser fabricated with this

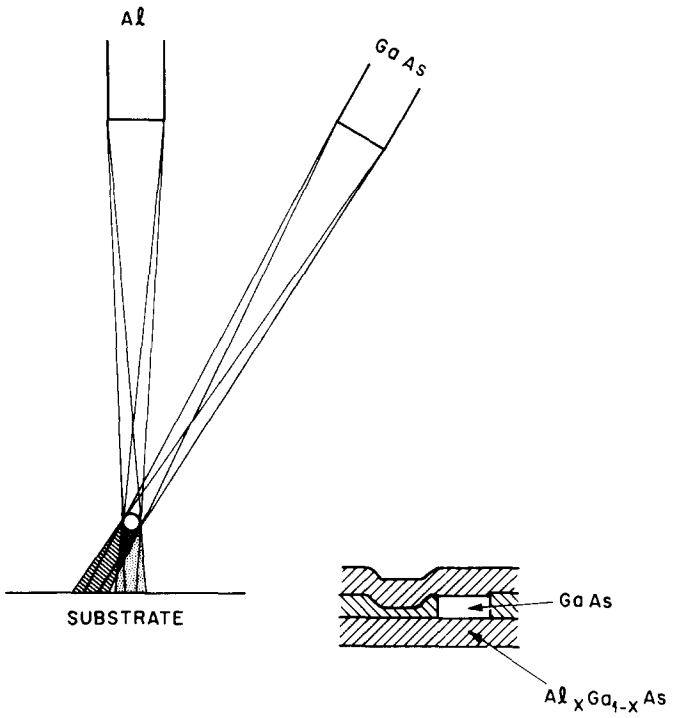

FIG. 34. Schematic of the experimental arrangement in an ultra-high-vacuum system to prepare three-dimensional dielectric waveguides. (Ref. 40.)

material. GaAs has an index of refraction equal to 3.54 and that of AlAs is 2.96. The index of refraction of $Al_xGa_{1-x}As$ decreases with increasing x with $\Delta = 0.2855x$ at 1.06 μm, where $\Delta = (n^2 - n_x^2)/n^2$, n is the index of refraction of GaAs and n_x is that of $Al_xGa_{1-x}As$.[130] For a small change in the AlAs mole fraction in the $Al_xGa_{1-x}As$, the index of refraction is therefore $n_x \approx n(1 - \Delta/2)$.

Three-dimensional dielectric waveguides for integrated optics have been prepared with MBE by a masking technique.[40] The schematic of the experimental arrangement is illustrated in Fig. 34. The masking is accomplished by a small-diameter wire in the beam path which shadows the Al beam in an area directly under the wire but allows the growth of GaAs in that area because the GaAs beam impinges from a different angle as shown in the figure. The growth of a rectangular pipe of GaAs surrounded by an $Al_xGa_{1-x}As$ medium was accomplished in three steps: (1) growth of an $Al_xGa_{1-x}As$ layer without the masking wire in place, (2) growth of second layer with the masking wire in place, and (3) growth of the third layer without the wire. The positioning of the wire was carried out through an air-to-vacuum manipulator so that the sample was not exposed to air between layer growth. Figure 35

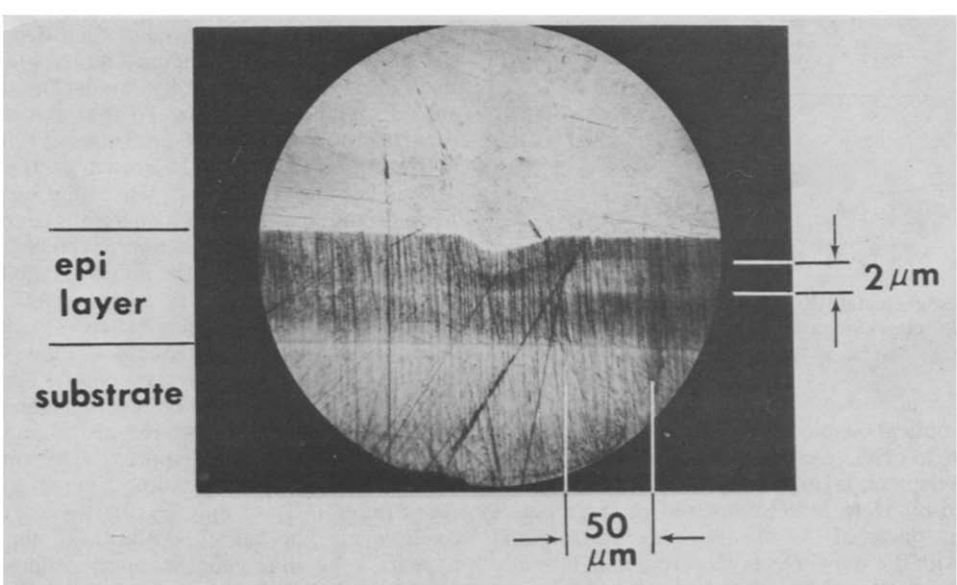

FIG. 35. Photomicrograph of the waveguide cross-section after angle lapping and staining.

is a photomicrograph of the cross section of the guide when the wafer was angle lapped and stained so as to show the guiding section.

Another approach to the fabrication of three-dimensional optical waveguides with MBE is through the use of the etching and regrowth technique.[131] Waveguides were made by first growing three epitaxial layers, $Al_xGa_{1-x}As$, GaAs, and $Al_xGa_{1-x}As$ on the {100} substrate. The layers were then removed from the growth system and etched off except for the area where the waveguide was to be formed. The waveguide area was protected from etching by oxide patterns formed using anodization and photolithographic techniques. The etched structure was then covered with another layer of $Al_xGa_{1-x}As$ by MBE to completely encapsulate the GaAs waveguide. The schematic diagram of the processing procedure in producing this three-dimensional GaAs light guide is shown in Fig. 36. Guides as small as 0.5×3 μm in cross section have been fabricated with this method. Preliminary evaluations showed that losses of less than 1 cm^{-1} can be achieved for guides having a layer thickness greater than 1 μm; losses increased over 5 cm^{-1} for layer thicknesses thinner than 0.7 μm. The increased loss for thin layers was probably due to interface scattering becoming important.

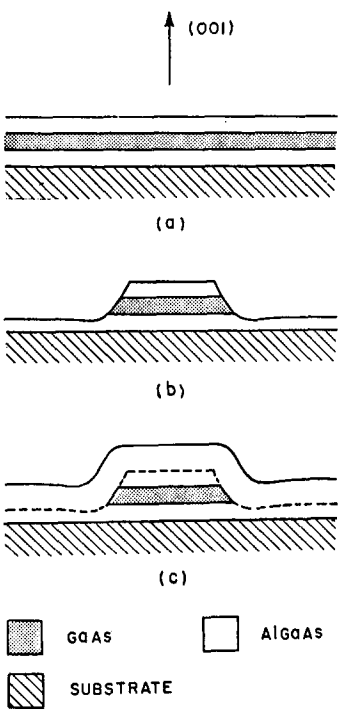

FIG. 36. Schematic diagram of processing steps in producing three-dimensional GaAs light guide in an $Al_xGa_{1-x}As$ cladding. (Ref. 131.)

Merz *et al.*[132] have described the preparation of tapered optical couplers by MBE. Tapered couplers are used to achieve efficient transfer of light from one waveguide layer to another. The structure prepared by Merz *et al.*, consisted of three layers ~ 1.5 μm thick of $Al_{0.3}Ga_{0.7}As$, $Al_{0.1}Ga_{0.9}As$, and GaAs, with the top GaAs layer terminated laterally by a linear taper ~ 200 μm wide. Light propagating in the GaAs layer was coupled by the taper into the $Al_{0.1}Ga_{0.9}As$ layer with nearly 100% efficiency, significantly greater than was obtained with similar structures grown by LPE.

VI. MBE planar technology

A significant factor in the present emphasis on Si as a device material has been the development of Si planar technology which is the basis for most integrated circuit processing. The formation of devices in selected areas through a SiO_2 masking layer is an important feature of this technology. The properties of GaAs, such as wide, direct bandgap and high electron mobility which make it desirable for high frequency and high temperature applications together with the availability of insulating monocrystalline GaAs substrate material, would seem to be good incentives for developing a comparable GaAs planar technology. Selected area growth of GaAs by chemical vapor deposition in holes etched through SiO_2 masks has been reported;[133-134] however, the growth occurs only in the etched windows, forming mesas, and there are problems with faceting and lateral growth overhanging the oxide.

Selected area growth can also be obtained using MBE, and the process has the interesting feature that while deposition occurs uniformly over the entire surface, epitaxial growth takes place only in the selected area.[120] The deposited layer elsewhere is polycrystalline with very high resistivity; it is effectively semi-insulating even when the epitaxial GaAs in the window area is doped *n*- or *p*-type as high as $10^{18}/cm^3$.[120] High resistivity in undoped polycrystalline GaAs deposited by either the three-temperature technique[135] or by MBE[136] at lower temperatures has been observed previously; Takahashi's measurements[135] indicated the presence of a deep trap 0.45 eV below the conduction band edge which is presumably associated with grain boundaries. The small grain size ~ 100 Å,[135] provides a high density of these traps.

Figure 37(a) shows an insulating GaAs substrate covered with a 2000 Å layer of SiO_2 deposited by the Silox process.[137] Rectangular windows have been opened in the oxide by standard photolithographic techniques. Figure 37(b) shows the same area after the growth of 6 μm GaAs at 570°C using MBE. It is evident that the growth on the window area is flat and featureless, while that on the SiO_2 has a texture indicative of a fine-grain structure. An enlarged, cleaved cross-section of the layer including the window area and the polycrystalline growth is shown in Fig. 37(c). The window area shows a featureless growth interface between the layer and substrate while the roughness of the fractured surface indicates the polycrystalline nature of the growth on the SiO_2 covered area. It can be seen that the window dimensions are preserved, and that the growth in the window is approximately level with the surrounding polycrystalline layer; the two surfaces differ in level only by the thickness of the oxide layer. The lateral resolution of the process appears to be quite good; monocrystalline areas as small as 5 μm across are visible in Fig. 37(b) where small alignment markers were etched through the

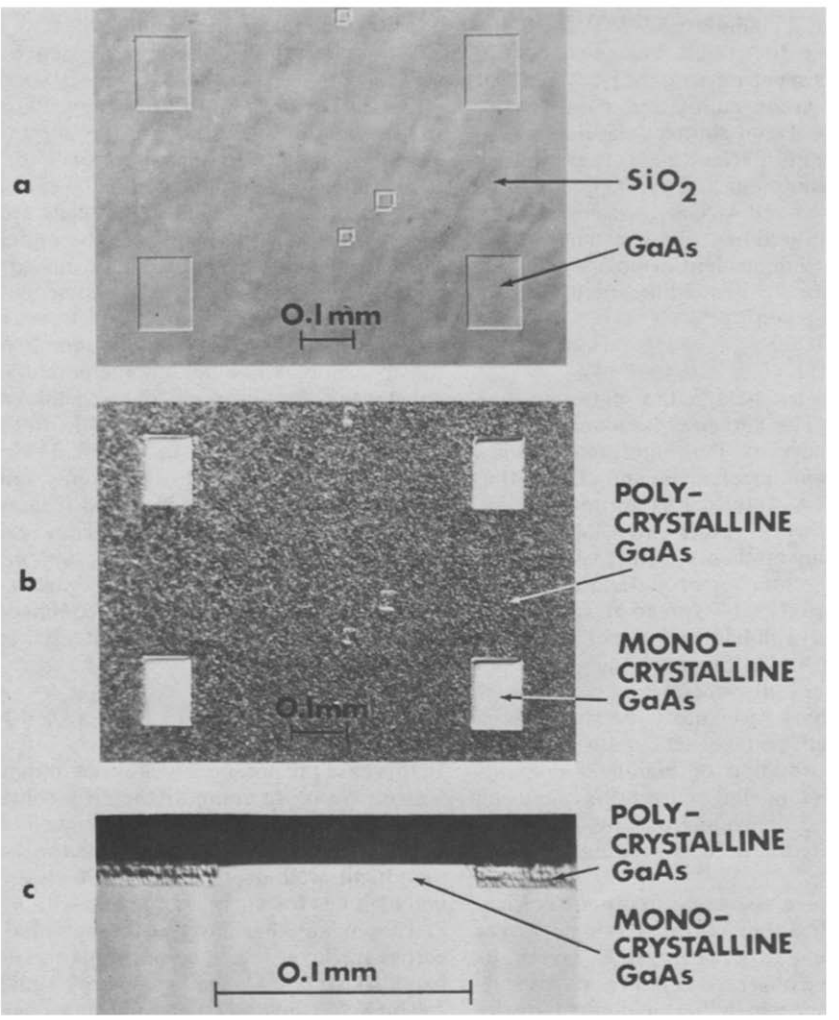

FIG. 37. Photomicrographs of (a) SiO_2 patterns on a Cr-doped GaAs substrate, (b) after depositing 6 μm of GaAs by MBE, (c) an enlarged view of the {110} cleaved cross-section of the wafer, showing monocrystalline featureless growth interface between the epitaxial layer and the substrate, and polycrystalline growth on SiO_2 film. (Ref. 120.)

original oxide. The epitaxial character of the large window areas was established by RED as well as by the cleavage.

The mixer diodes discussed in Section V-C were fabricated on selected area growth films similar to the one shown in Fig. 37. Since the surrounding areas were insulating, it was possible to deposit the gold beam-leads directly on the polycrystalline GaAs surface, thus simplifying the processing procedure considerably. The insulating character of the substrate and polycrystalline film greatly reduced the parasitic capacitance between beam-leads and substrate, making high-frequency operation possible with devices which are compatible with beam-lead technology.

It is anticipated that the ability to produce electrically isolated, planar epitaxial structures of GaAs with well-defined geometry will find many applications. The prospect of GaAs integrated circuit fabrication by MBE now seems likely. Furthermore, the results of Davey and Pankey[138] and Arthur and Morris[136] on polycrystalline GaP films which also exhibited resistivities $>10^6\,\Omega$ cm suggest that MBE selected area growth may be possible with GaP as well.

VII. Research applications of MBE

A. *Periodic structures*

Periodic structures consist of alternate thin layers of monocrystalline materials of different compositions. The term superlattice is used to denote a structure with period less than the electron mean free path. Esaki and Tsu analyzed the dynamics of electrons traversing the resulting periodic potential, and predicted a range of velocities where negative resistance would occur.[139] Until the development of MBE it was difficult to test their theory since structures with a small enough period could not be obtained, nor was the problem of interfacial electronic states adequately resolved.

Superlattice structures have now been prepared by computer-controlled MBE by Chang *et al.*[3, 39, 140] in which there are typically 100 periods with each

period consisting of a GaAs layer ~60 Å thick and a $Ga_{0.5}Al_{0.5}As$ layer ~10 Å thick. Thickness control is obtained by mass spectrometric measurements of beam flux which are used by the computer to determine when the beam shutters should be activated. The absence of interface states is assured by the clean growth conditions and by the good lattice match between GaAs and $Al_xGa_{1-x}As$. These structures have demonstrated negative resistance above ~2 v bias which is independent of polarity. In fact the threshold electric field is within a factor of 2 of the predicted field given by

$$eE\tau d/\hbar \sim 1$$

where E is the electric field, τ the scattering time and d the period. The agreement between theory and measurement supports their interpretation of a superlattice dispersion mechanism and implies that the GaAs–$Al_xGa_{1-x}As$ interface is abrupt.

In more recent work Esaki and Chang[141] describe a comparison of theory with experimental results from a large number of superlattices with three different periods; the spread of their data indicates a range of well widths for each period of no more than 5–7 Å. In this work they also described low-temperature conductance measurements showing sharp oscillatory behavior as a function of applied voltage. They attribute this behavior to the formation of high-field domains across which the tunneling current is a strong function of the field depending on how the quantized energy levels in adjacent potential wells overlap.

Chang *et al.*[142] have also measured the electrical conductance of ultra-thin (40–50 Å) single layers of GaAs sandwiched between 80 Å layers of $Al_{0.7}Ga_{0.3}As$ and have observed field-dependent variations in conductance which they attribute to resonant tunneling through quantized energy states in the GaAs layer. Negative resistance was observed in narrow regions centered about −0.53 volts and +0.79 volts; this polarity dependence indicated some asymmetry in the $Al_{0.7}Ga_{0.3}As$ barriers.

Optical absorption spectroscopy is a somewhat simpler method for studying the energy levels of electrons confined to thin layers since the problems of making ohmic contacts to thin layers and electric field distortion of the potential wells are avoided. Dingle *et al.*[143] have measured the optical absorption in structures comprised of up to fifty thin GaAs layers (70–4000 Å) sandwiched between $Al_{0.2}Ga_{0.8}As$ layers >250 Å thick. The reason for the large number of GaAs layers was simply to enhance the absorption while holding the potential well size constant. They observed for each thickness up to 500 Å a series of well-defined peaks in the absorption spectrum as shown in Fig. 38. Their measurements were restricted to the energy range below 1.75 eV since absorption in the $Al_{0.2}Ga_{0.8}As$ became significant at higher energies. They explain this spectrum as due to the absorption of excitons associated with electron and hole states quantized in one dimension. For a particle confined to a layer of thickness L_Z by an infinite potential barrier, the energy levels are

$$E = \left(\frac{\hbar^2}{2m}\right)\left[(k_x^2 + k_y^2) + \left(\frac{\pi n}{L_Z}\right)^2\right], \quad n = 1, 2, 3\ldots$$

In this case the potential well is not infinite so that it was necessary to compute the eigenvalues numerically for various values of the well depth. An excellent fit to the data was obtained with a conduction band well depth of 220 ± 30 meV, including bound states for the thicker layers with n as high as 7. This means that most of the potential variation across the layer interface occurs in the conduction band since the bandgap energy difference is 250 meV for the two compounds used here. Confirmation of this was obtained from the slight splitting of the $n = 1$ peak for the thinnest films which

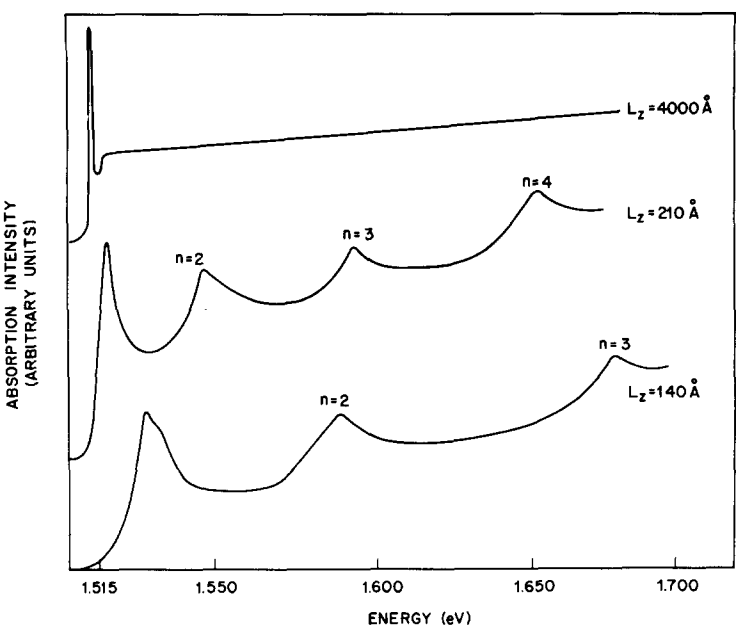

FIG. 38. Absorption spectra at 2 K for $Al_xGa_{1-x}As$–GaAs–$Al_xGa_{1-x}As$ heterostructures of various thicknesses. (Ref. 143.)

indicated that the valence band potential variation is ~ 30 meV. When attempts were made to fit the data with eigenvalues calculated for non-rectangular potential wells, it was evident that the potential variation occurs in less than 5 Å. This is further evidence first, for the remarkable abruptness of GaAs–$Al_x Ga_{1-x}$ As interfaces, and second, for the even more remarkable uniformity in thickness obtained over as many as fifty layers.

B. *Surface studies*

For many surface experiments, the preparation of a flat, ordered, clean surface is an important prerequisite. Such experiments would include LEED, ellipsometry and electron energy-loss spectroscopy (ELS). It has already been pointed out that ordering of the surface into the various different structures has become reproducible only with the use of MBE. Such surfaces will be essential for the complete LEED structural analyses of the future.

Ludeke and Esaki[144] have used MBE to prepare Ga-stabilized GaAs($\bar{1}\bar{1}\bar{1}$)–$\sqrt{19}$ and As-stabilized ($\bar{1}\bar{1}\bar{1}$)–2 surfaces for ELS. This type of measurement is convenient to make in the MBE apparatus described in Section II using the Auger electron spectrometer.[145,146] Ludeke and Esaki observed structure in the ELS spectrum for the ($\bar{1}\bar{1}\bar{1}$)–2–(As) surface at 1.7 eV which they attribute to transitions from filled surface states to conduction band states. This structure disappeared when the surface was converted to ($\bar{1}\bar{1}\bar{1}$)–$\sqrt{19}$–(Ga). They compared these results with ELS results from both annealed and sputtered Ge[111] surfaces, on which they observed similar structure at 1.7 eV on the sputtered surface but not on the annealed surface. They argued that sputtering should introduce "dangling bond" surface states which would also be present on GaAs containing an excess of As. Whether or not this interpretation is substantiated, their results show the value in being able to alter the surface composition in a well-defined manner.

VIII. Concluding remarks

In this review we have described the technique for epitaxial growth of III–V compounds now known as Molecular Beam Epitaxy. Because it is an unconventional technique in its reliance on multiple *in-situ* methods of surface characterization, we have discussed the experimental procedures of MBE in some detail. Our understanding of the general mechanism of MBE, gained from morphological studies and kinetic measurements, while still incomplete is probably better than that for more conventional growth techniques, simply because of the ability to study the surface while growth is occurring. Admittedly, our understanding of the incorporation of impurities leaves much to be desired, since it is not clear whether the process is governed by thermodynamic or kinetic parameters. Nevertheless, a sufficient amount of empirical data on dopants exists that it is possible to grow layers doped *n*- or *p*-type from 10^{16} to $10^{19}/cm^3$.

As we have emphasized throughout, the real strength of MBE lies in the control which it allows over thickness and composition. The optical absorption results of Dingle *et al.*[143] indicate that a reproducible thickness control of < 5 Å is achieved during the growth of a large number of layers. Since certain semiconductor devices require this kind of control for optimum performance; there is clearly a future for MBE in device fabrication. There is also an important application for MBE in fundamental studies, either for the preparation of flat, ordered surfaces of controlled composition or for the growth of abrupt interfaces and very thin layers.

The development of an MBE planar technology provides a means for controlled growth parallel to the surface as well as normal to it. Since polycrystalline deposits of both GaAs and GaP exhibit the high resistivity needed for device isolation, it seems likely that this technology will be applicable to a range of compositions of binary and ternary III–V compounds.

Finally, we should emphasize that while the discussion has been concerned only with III–V compounds, there is much evidence in the literature that a similar approach will apply to II–VI and IV–VI compounds. An investigation of vapor pressures, sticking coefficients and surface compositions of the II–VI compounds is underway[147] and MBE layers of several compounds have been grown. Progress will undoubtedly be rapid.

Acknowledgments

We should like to thank our colleagues M. B. Panish, M. Ilegems, H. C. Casey, R. E. Dingle, A. C. Gossard and W. Weigmann for helpful discussion and new results, and C. Radice and J. J. LePore for excellent technical assistance.

References

1. A. Y. Cho, M. B. Panish and I. Hayashi, *Proc. Symp. GaAs and Related Compounds, Aachen, Germany, 1970*, p. 18, Institute of Physics, London, 1971.
2. A. Y. Cho, *Appl. Phys. Lett.* **19**, 467 (1971).
3. L. L. Chang, L. Esaki, W. E. Howard and R. Ludeke, *J. Vac. Sci. Technol.* **10**, 11 (1973).
4. D. W. Shaw, *J. Electronic Materials*, **2**, 255 (1973).
5. M. B. Panish and I. Hayashi in *Applied Solid State Science*, vol. 4, p. 236, ed. by R. Wolfe, Academic Press, Inc., New York, 1974.
6. Karl-Georg Günther in *Compound Semiconductors*, vol. I, p. 313, ed. by R. K. Willardson and H. L. Goering, Reinhold Publishing Corporation, New York, 1961.
7. C. Paparoditis, *ibid.*, p. 326.
8. L. I. Maissel and M. H. Francombe, *An Introduction to Thin Films*, Gordon & Breach, New York, 1973.
9. H. H. Wieder, *Intermetallic Semiconducting Films*, Pergamon Press, Braunschweig, 1970.
10. B. A. Joyce, *Rep. Prog. Phys.* **37**, 363 (1974).
11. B. Lewis, *Thin Solid Films*, **7**, 179 (1971).
12. H. M. Manasevit, *J. Crystal Growth*, **22**, 125 (1974).
13. B. E. Watts, *Thin Solid Films*, **18**, 1 (1973).
14. T. L. Chu and R. K. Smeltzer, *J. Vac. Sci. Technol.* **10**, 1 (1973).
15. J. N. Zemel, in *Solid State Surface Science*, vol. I, p. 291, ed. by M. Green, Marcel Dekker, New York, 1969.

16. A. J. ELLEMAN and H. WILMAN, *Proc. Phys. Soc. (Lond.)* **61**, 164 (1948).
17. R. B. SCHOOLAR and J. N. ZEMEL, *J. Appl. Phys.* **35**, 1848 (1964).
18. R. F. BREBRICK and A. J. STRAUSS, *J. Chem. Phys.* **40**, 3230 (1964).
19. J. R. ARTHUR and A. G. CULLIS, unpublished results.
20. J. L. RICHARDS, P. B. HART and L. M. GALLONE, *J. Appl. Phys.* **34**, 3418 (1963).
21. J. L. RICHARDS, P. B. HART and E. K. MUELLER in *Single-crystal Films*, p. 241, ed. by M. H. FRANCOMBE and H. SATO, Pergamon Press, New York, 1964.
22. R. J. COLLINS, F. W. REYNOLDS and G. W. STILWELL, U.S. Patent no. 2,759,861 (1956).
23. K. G. GÜNTHER, *Z. Naturforsch.* A, **13a**, 1081 (1958).
24. D. HANEMAN, *J. Phys. Chem. Solids*, **14**, 162 (1960).
25. D. HANEMAN, *Phys. Rev.* **121**, 1093 (1961).
26. H. E. FARNSWORTH, R. E. SCHLIER, M. GEORGE and R. M. BURGER, *J. Appl. Phys.* **26**, 252 (1955).
27. J. J. UEBBING and N. J. TAYLOR, *J. Appl. Phys.* **41**, 804 (1970).
28. J. T. GRANT and T. W. HASS, *J. Vac. Sci. Technol.* **8**, 94 (1971).
29. H. HOLLOWAY, J. L. RICHARDS, L. C. BOBB and J. PERRY, *J. Appl. Phys.* **37**, 4694 (1966).
30. J. E. DAVEY and T. PANKEY, *J. Appl. Phys.* **39**, 1941 (1968).
31. J. R. ARTHUR, *J. Appl. Phys.* **39**, 4032 (1968).
32. J. R. ARTHUR and J. J. LEPORE, *J. Vac. Sci. Technol.* **6**, 546 (1969).
33. A. Y. CHO, *J. Appl. Phys.* **41**, 782 (1970).
34. A. Y. CHO and Y. S. CHEN, *Solid State Commun.* **8**, 377 (1970).
35. A. Y. CHO and M. B. PANISH, *J. Appl. Phys.* **43**, 5118 (1972).
36. J. R. ARTHUR, *Surf. Sci.* **38**, 394 (1973).
37. A. Y. CHO, *J. Appl. Phys.* **42**, 2074 (1971).
38. D. B. DOVE, R. LUDEKE and L. L. CHANG, *J. Appl. Phys.* **44**, 1897 (1973).
39. L. L. CHANG, L. ESAKI, W. E. HOWARD, R. LUDEKE and G. SCHUL, *J. Voc. Sci. Technol.* **10**, 655 (1973).
40. A. Y. CHO and F. K. REINHART, *Appl. Phys. Lett.* **21**, 355 (1972).
41. C. T. FOXON, M. R. BOUDRY and B. A. JOYCE, *Surf. Sci.* **44**, 69 (1974).
42. C. T. FOXON, *Acta Electron.* **16**, 323 (1973).
43. J. R. ARTHUR, *J. Phys. Chem. Solids*, **28**, 2257 (1967).
44. C. T. FOXON, J. A. HARVEY and B. A. JOYCE, *J. Phys. Chem. Solids*, **34**, 1693 (1973).
45. C. D. THURMOND, *J. Phys. Chem. Solids*, **26**, 785 (1965).
46. W. R. KNOLLE, unpublished.
47. L. BREWER and J. S. KANE, *J. Phys. Chem.* **59**, 105 (1955).
48. A. Y. CHO and F. K. REINHART, *J. Appl. Phys.* **45**, 1812 (1974).
49. C. C. CHANG, *Surf. Sci.* **25**, 53 (1971).
50. J. C. TRACY in *Electron Emission Spectroscopy*, ed. by W. DEKEYSER *et al.*, D. Reidel Publishing Company, Dordrecht-Holland, 1973.
51. P. W. PALMBERG in *Electron Spectroscopy*, ed. by D. A. SHIRLEY, North-Holland, Amsterdam, 1972.
52. J. R. ARTHUR, *J. Appl. Phys.* **38**, 4023 (1967).
53. B. A. JOYCE, J. H. NEAVE and B. E. WATTS, *Surf. Sci.* **15**, 1 (1969).
54. B. A. JOYCE, *Rep. Prog. Phys.* **37**, 363 (1974).
55. E. W. JENSEN, *Solid State Technol.*, Aug. 1973, pp. 49–52.
56. A. U. MACRAE, *Surface Sci.* **4**, 247 (1966).
57. B. A. JOYCE and J. H. NEAVE, *Surface Sci.* **34**, 401 (1973).
58. R. LUDEKE, L. ESAKI and L. L. CHANG, *Appl. Phys. Lett.* **24**, 417 (1974).
59. A. Y. CHO and I. HAYASHI, *Solid-State Electron*, **14**, 125 (1971).
60. F. JONA, *IBM J. Res. Develop.* **9**, 375 (1965).
61. A. U. MACRAE and G. W. GOBELI, *J. Appl. Phys.* **35**, 1629 (1964).
62. J. M. CHEN, *Surf. Sci.* **25**, 305 (1971).
63. P. J. ESTRUP and E. G. MCRAE, *Surf. Sci.* **25**, 1 (1972).
64. E. BAUER, Reflection electron diffraction. In *Techniques of Metals Research*, vol. 2, p. 501, ed. by R. F. BUNSHAW New York, Interscience, 1969.
65. E. BAUER, Low-energy electron diffraction. *Ibid.*, p. 559.
66. C. B. DUKE, Electron scattering by solids: determination of the chemical, geometrical, electronic and vibrational structure of surfaces. In *Electron Emission Spectroscopy*, ed. by W. DEKEYSER *et al.*, D. Reidel Publishing Company, Dordrecht-Holland, 1973.
67. C. B. DUKE, N. O. LIPARI and G. E. LARAMORE, *J. Vac. Sci. Technol.* **11** (1974).
68. A. Y. CHO, *J. Vac. Sci. Technol.* **8**, S31 (1971).
69. E. A. WOOD, *J. Appl. Phys.* **35**, 1306 (1964).
70. A. Y. CHO, *J. Appl. Phys.* **41**, 2780 (1970).
71. J. R. ARTHUR, unpublished results.
72. J. J. UEBBING and N. J. TAYLOR, *J. Appl. Phys.* **41**, 804 (1970).
73. E. BAUER, *Phys. Lett.* A, **26**, 530 (1968).
74. N. J. TAYLOR, *Surf. Sci.* **15**, 169 (1969).
75. R. W. NOSKER, P. MARK and J. D. LEVINE, *Surf. Sci.* **19**, 291 (1970).
76. P. MARK, *J. Vac. Sci. Technol.* **10**, 893 (1973).
77. Cliftronics SE-3K/5U, Clifton, N. J.
78. D. B. DOVE, R. LUDEKE and L. L. CHANG, *J. Appl. Phys.* **44**, 1897 (1973).
79. H. C. ABBINK, R. M. BROUDY and G. P. MCCARTHY, *J. Appl. Phys.* **39**, 4673 (1968).
80. W. K. BURTON, N. CABRERA and F. E. FRANK, *Phil. Trans. Roy. Soc.* A, **243**, 299 (1950).
81. J. R. ARTHUR, *Surf. Sci.* **43**, 449 (1974).
82. H. SHELTON and A. Y. CHO, *J. Appl. Phys.* **37**, 3544 (1966).
83. J. B. HUDSON and J. S. SANDEJAS, *Surf. Sci.* **15**, 27 (1969).
84. A. Y. CHO and C. D. HENDRICKS, *J. Appl. Phys.* **40**, 339 (1969).
85. R. J. H. VOORHOEVE and R. S. WAGNER, *J. Appl. Phys.* **42**, 3948 (1971).
86. R. J. H. VOORHOEVE, J. N. CARIDES and R. S. WAGNER, *J. Appl. Phys.* **43**, 4876 (1972).
87. T. T. A. NGUYEN, R. CINTI and B. K. CHAKRAVERTY, *J. Cryst. Growth*, **13–14**, 174 (1972).
88. A. Y. CHO and I. HAYASHI, *J. Appl. Phys.* **42**, 4422 (1971).
89. J. R. ARTHUR, unpublished results.
90. A. Y. CHO and I. HAYASHI, *Met. Trans.* **2**, 777 (1971).
91. A. Y. CHO and H. C. CASEY, Jr., *J. Appl. Phys.* **45**, 1258 (1974).
92. A. Y.CHO, to be published in *J. Appl. Phys.* April (1975).
93. M. ILEGEMS and R. DINGLE, *Proc. Symp. GaAs and Related Compounds, Deauville, France, 1974*, Inst. of Phys. London, 1975.
94. K. J. MATYSIK, R. J. H. VOORHOEVE and J. N. CARIDES, *J. Vac. Sci. Technol.* **11**, 493 (1974).
95. D. L. RODE and S. KNIGHT, *Phys. Rev.* **B, 3**, 2534 (1971).
96. C. J. HWANG, *Phys. Rev.* **180**, 827 (1969).
97. E. W. WILLIAMS and C. T. ELLIOTT, *Brit. J. Appl. Phys.* **2**, 1657 (1969).

98. J. A. ROSSI, C. M. WOLF, G. E. STILLMAN and J. O. DIMMOCK, *Solid State Commun.* **8**, 2021 (1970).
99. D. D. SELL, S. E. STOKOWSKI, R. DINGLE and J. V. DILORENZO, *Phys. Rev.* B, **7**, 4568 (1973).
100. H. C. CASEY, Jr. and R. H. KAISER, *J. Electrochem. Soc.* **114**, 149 (1967).
101. B. TUCK, *Phys. Stat. Sol.* **36**, 285 (1969).
102. E. W. WILLIAMS and D. M. BLACKNALL, *Trans. Metall. Soc. of AIME*, **239**, 387 (1967).
103. D. F. NELSON, M. GERSHENZON, A. ASHKIN, L. A. D'ASARO and T. C. ARACE, *Appl. Phys. Lett.* **2**, 182 (1963).
104. A. Y. CHO and H. C. CASEY, Jr., *Appl. Phys. Lett.* **25**, 288 (1974).
105. H. C. CASEY, Jr., A. Y. CHO and P. A. BARNES, to be published in *IEEE Quantum Electron.*
106. T. M. DONOVAN, E. J. ASHLEY and H. E. BENNETT, Jr., *J. Opt. Soc. Am.* **53**, 1403 (1963).
107. D. D. SELL and A. U. MCRAE, *J. Appl. Phys.* **41**, 4927 (1970).
108. The notations were assigned by M. CARDONA; see, for example, *Solid State Physics*, ed. by F. SEITZ, D. TURNBULL and H. EHRENREICH, Suppl. vol. 11, Academic Press, New York, 1969.
109. D. D. SELL, *Appl. Opt.* **9**, 1926 (1970).
110. S. E. STOKOWSKI and A. Y. CHO, unpublished.
111. S. M. SZE, *Physics of Semiconductor Devices*, Wiley, New York, 1969.
112. J. A. COPELAND, *IEEE Trans. Electron. Devices*, ED-**16**, 445 (1969).
113. W. T. READ, Jr., *Bell Syst. Tech. J.* **37**, 401 (1958).
114. G. SALMER, J. PRIBETICH, A. FARRAYRE and B. KRAMER, *J. Appl. Phys.* **44**, 314 (1973).
115. J. C. IRVIN, *Proc. Fourth Biennial Cornell Electronic Engineering Conference*, p. 287. Cornell U.P., Ithaca, N.Y., 1973.
116. C. K. KIM, W. G. MATTHEI and R. STEELE, in ref. 115, p. 299.
117. A. Y. CHO, C. N. DUNN, R. L. KUVAS and W. E. SCHROEDER, *Appl. Phys. Lett.* **25**, 224 (1974).
118. I. TATSUGUCHI, N. R. DIETRICH and C. B. SWAN, *IEEE Solid State Circuit*, Sc-7, 2 (1972).
119. R. L. KUVAS, *IEEE Trans. Electron. Devices*, ED-**19**, 220 (1972).
120. A. Y. CHO and W. C. BALLAMY, *J. Appl. Phys.* **46**, 783 (1975).
121. W. C. BALLAMY and A. Y. CHO, to be published.
122. G. S. AXELING, unpublished.
123. The metallization and electrical measurements were performed by R. F. BAIR, J. S. HAYES and W. M. ROSSER.
124. L. S. NAPOLI, J. J. HUGHES, W. F. REICHERT and S. JOLLY, *RCA Rev.* **34**, 608 (1973).
125. R. B. FAIR, J. S. HAYES and W. M. ROSSER, unpublished.
126. I. HAYASHI, M. B. PANISH, P. W. FOY and S. SUMSKI, *Appl. Phys. Lett.* **17**, 109 (1970).
127. ZH. I. ALFEROV, V. M. ANDREEV, D. Z. GARBUZO, YU. V. ZHILGAEV, E. P. MOROZOV, E. L. PORTNOI and V. G. TROFIM, *Fiz. Tekh. Poluprov.* **4**, 1826 (1970).
128. I. HAYASHI, B. M. PANISH and F. K. REINHART, *J. Appl. Phys.* **42**, 1929 (1971).
129. A. Y. CHO and S. E. STOKOWSKI, *Solid State Commun.* **9**, 565 (1971).
130. F. K. REINHART, private communication.
131. J. C. TRACY, W. WIEGMANN, R. A. LOGAN and F. K. REINHART, *Appl. Phys. Lett.* **22**, 511 (1973).
132. J. L. MERZ, R. A. LOGAN, W. WIEGMANN and A. C. GOSSARD, to be published.
133. D. W. SHAW, *J. Electrochem. Soc.* **113**, 904 (1966).
134. D. W. SHAW, *J. Electrochem. Soc.* **115**, 777 (1968).
135. K. TAKAHASI, *J. Vac. Sci. Technol.* **9**, 502 (1972).
136. J. R. ARTHUR, Jr. and F. J. MORRIS, U.S. Patent 3,666,553 (1972).
137. Silox is a commercial trade name for an oxidation system which can deposit SiO_2 films by the oxidation of silane at 250° to 450°C. Silox is manufactured by Applied Materials Technology, Inc., 2999 San Ysidro Way, Santa Clara, CA 95051.
138. J. E. DAVEY and T. PANKEY, *J. Appl. Phys.* **40**, 212 (1969).
139. L. ESAKI and R. TSU, *IBM J. Res. Develop.* **14**, 61 (1970).
140. L. ESAKI, *Proc. 5th Conf. on Solid State Devices, Tokyo, 1973.* (Supplement to the *J. Japan Soc. Appl. Phys.* **43**, 452 (1974).)
141. L. ESAKI and L. L. CHANG, *Phys. Rev. Lett.* **33**, 495 (1974).
142. L. L. CHANG, L. ESAKI and R. TSU, *Appl. Phys. Lett.* **24**, 593 (1974).
143. R. DINGLE, W. WIEGMANN and C. H. HENRY, *Phys. Rev. Lett.* **33**, 827 (1974).
144. R. LUDEKE and L. ESAKI, *Phys. Rev. Lett.* **33**, 653 (1974).
145. E. SICKAFUS and F. STEINRISSER, *Phys. Rev.* B, **6**, 3714 (1972).
146. J. E. ROWE and H. IBACH, *Phys. Rev. Lett.* **31**, 102 (1973).
147. D. L. SMITH, ARPA Contract no. N00014-73-0280. Reports of March 25, 1974 and June 30, 1974.

Appendix

Bibliography of MBE

In this section the authors and titles of publications related to MBE are listed chronologically. Since prior to 1964 the evaporated films were usually polycrystalline, we have included only a representative selection of papers for this period. A more complete bibliography of the early work is given by Wieder.[9] For the period after 1964 we have included only papers in which epitaxial growth was clearly established and growth occurred by processes closely related to the present MBE technique. Also included are papers in which MBE grown films are analyzed or used in devices or experiments which are indicative of their material properties. Our choice of papers is thus rather arbitrary and undoubtedly incomplete for materials other than III–V compounds.

Appendix

Early work—polycrystalline films

A. J. ELLEMAN and H. WILMAN, The structure and growth of PbS deposits on rocksalt substrates. *Proc. Phys. Soc. (Lond.)* **61**, 164 (1948).
R. J. COLLINS, F. W. REYNOLDS and G. R. STILWELL, Electrical and optical properties of GaSb films. *Phys. Rev.* **98**, 227 (1955).
R. J. COLLINS, F. W. REYNOLDS and G. R. STILWELL, Photoconducting, semiconducting compounds of elements of groups III and V. U.S. Patent no. 2,759,861 (1956).
K. G. GÜNTHER, Thin layers of III–V compounds. U.S. Patent no. 2,938,816 (1956).
K. G. GÜNTHER, Evaporated layers of semiconducting III–V compounds. *Naturwissenshaften*, **45**, 415 (1958).

W. HÄNLEIN and K. G. GÜNTHER, Preparation and properties of compound-layers by vacuum deposition. In *Advances in Vacuum Science and Technology*, vol. II, p. 727, Pergamon Press, New York, 1960.
C. PAPARODITIS, Preparation and properties of thin films of semiconducting intermetallic compounds obtained by vacuum evaporation. In *Solid State Physics in Electronics and Telecommunications*, Academic Press, New York, 1960.
R. F. POTTER and GEORGE G. KRETSCHMAR, Optical properties of evaporated InSb films. *J. Opt. Soc. Am.* **51**, 693 (1961).
R. P. HOWSON, The preparation and study of the optical absorption edge of thin films of gallium arsenide. *J. de Phys.* **25**, 212 (1964).
S. MARTINUZZI, M. PERROT and J. FOURNY, Preparation et propriétés optiques de couches minces d'arseniure de gallium et de tellurure de cadmium. *J. de Phys.* **25**, 203 (1964).

1964—Epitaxial films

R. B. SCHOOLAR and J. N. ZEMEL, Preparation of single-crystal films of PbS. *J. Appl. Phys.* **35**, 1848 (1964).

1965

J. N. ZEMEL, J. D. JENSEN and R. B. SCHOOLAR, Electrical and optical properties of epitaxial films of PbS, PbSe, PbTe, and SnTe. *Phys. Rev.* **140** A, 330 (1965).

1966

H. HOLLOWAY, J. L. RICHARDS, L. C. BOBB and J. PERRY, Jr., Oriented growth of semiconductors IV. Vacuum deposition of epitaxial indium antimonide. *J. Appl. Phys.* **37**, 4694 (1966).
R. F. STEINBERG and D. M. SCRUGGS, Preparation of epitaxial GaAs films by vacuum evaporation of the elements. *J. Appl. Phys.* **37**, 4586 (1966).

1967

R. F. EGERTON and C. JUHASZ, Epitaxial films of PbTe, PbSe, and PbS grown on mica substrates. *Brit. J. Appl. Phys.* **18**, 1009 (1967).

1968

J. R. ARTHUR, Interaction of Ga and As_2 molecular beams with GaAs surfaces. *J. Appl. Phys.* **39**, 4032 (1968).
JOHN E. DAVEY and TITUS PANKEY, Epitaxial GaAs films deposited by vacuum evaporation. *J. Appl. Phys.* **39**, 1941 (1968).
R. F. STEINBERG, Photoemission from GaAs thin films. *Appl. Phys. Lett.* **12**, 63 (1968).

1969

J. R. ARTHUR, Interaction of As_2, P_2 and Bi molecular beams with GaAs and GaP $(\bar{1}\bar{1}\bar{1})$ surfaces. In *The Structure and Chemistry of Solid Surfaces*, p. 46-1, ed. by G. A. SOMERJAI, Wiley, New York, 1969.
J. R. ARTHUR and J. J. LEPORE, GaAs, GaP, and $GaAs_xP_{1-x}$ epitaxial films grown by molecular beam depositions. *J. Vac. Sci. Technol.* **6**, 545 (1969).
A. Y. CHO, Epitaxy by periodic annealing. *Surf. Sci.* **17**, 494 (1969).
D. L. SCHAEFER, A technique for evaporating films of alloys of III–V compounds by a three-temperature method. *Rev. Sci. Instr.* **40**, 1649 (1969).

1970

R. F. BIS, Electrical properties of $Pb_xSn_{1-x}Te$ alloys. *J. Vac. Sci. Technol.* **7**, 126 (1970).
A. Y. CHO and Y. S. CHEN, Epitaxial growth and optical evaluation of gallium phosphide and gallium arsenide thin films on calcium fluoride substrate. *Solid State Commun.* **8**, 377 (1970).
A. Y. CHO, Epitaxial growth of gallium phosphide on cleaved and polished (111) calcium fluoride. *J. Appl. Phys.* **41**, 782 (1970).
A. Y. CHO, Morphology of epitaxial growth of GaAs by a molecular beam method: the observation of surface structures. *J. Appl. Phys.* **41**, 2780 (1970).
P. J. DEASLEY, S. J. T. OWEN and P. W. WEBB, The growth and properties of epitaxial layers of zinc sulphide on germanium. *J. Mater. Sci.* **5**, 1054 (1970).
T. O. FARINRE and J. N. ZEMEL, Preparation and properties of $Pb_{1-x}Sn_xTc$ epitaxial films. *J. Vac. Sci. Technol.* **7**, 121 (1970).
J. W. WAGNER and A. G. THOMPSON, Growth and characterization of lead telluride epitaxial layers. *J. Electrochem. Soc.* **117**, 936 (1970).

1971

J. R. ARTHUR, Technique for growth of epitaxial compound semiconductor films. U.S. Patent no. 3,615,931 (1971).
A. Y. CHO and I. HAYASHI, Surface structures and photoluminescence of molecular beam epitaxial films of GaAs. *Solid-State Electronics*, **14**, 125 (1971).
A. Y. CHO, M. B. PANISH and I. HAYASHI, Molecular beam epitaxy of GaAs, $Al_xGa_{1-x}As$ and GaP. *Proc. Symp. GaAs and Related Compounds, Aachen, Germany, 1970*, p. 18, Institute of Physics, London, 1971.
A. Y. CHO and I. HAYASHI, Epitaxy of silicon doped gallium arsenide by molecular beam method. *Metall. Trans.* **2**, 777 (1971).
A. Y. CHO, GaAs epitaxy by a molecular beam method: observation of surface structure on the (001) face. *J. Appl. Phys.* **42**, 2074 (1971).
A. Y. CHO and S. E. STOKOWSKI, Molecular beam epitaxy and optical evaluation of $Al_xGa_{1-x}As$. *Solid State Commun.* **9**, 565 (1971).
A. Y. CHO, Film deposition by molecular beam techniques. *J. Vac. Sci. Technol.* **8**, S31 (1971).
A. Y. CHO and I. HAYASHI, *P–N* junction formation during molecular beam epitaxy of Ge-doped GaAs. *J. Appl. Phys.* **42**, 4422 (1971).
A. Y. CHO, Growth of periodic structures by the molecular-beam method. *Appl. Phys. Lett.* **19**, 467 (1971).
J. E. GENTHE and R. E. ALDRICH, Vacuum deposition of epitaxial ZnSe on GaAs. *Thin Solid Films*, **8**, 149 (1971).
R. LUDEKE, A survey of optical and electrical properties of thin films of II–VI semiconducting compounds. *J. Vac. Sci. Technol.* **8**, 199 (1971).
R. B. SCHOOLAR and J. R. LOWNEY, Photoconductive PbSe epitaxial films. *J. Vac. Sci. Technol.* **8**, 224 (1971).
G. SHIMAOKA, Structure and epitaxy of evaporated cadmium sulfide films. *Thin Solid Films*, **7**, 405 (1971).
G. YAN and L. YOUNG, Structural and electrical properties of sublimed GaAs films. *Solid-State Electron.* **14**, 1003 (1971).

1972

R. F. BIS, J. R. DIXON and J. R. DOWNEY, Thick epitaxial films of $Pb_{1-x}Sn_xTe$. *J. Vac. Sci. Technol.* **9**, 226 (1972).
J. T. CALOW, D. L. KIRK and S. J. T. OWEN, The growth of epitaxial ZnSe upon germanium substrates. *Thin Solid Films*, **9**, 409 (1972).

A. CEPEDA, G. MCLANE and J. N. ZEMEL, Sorption effects on epitaxic PbSe films. *J. Vac. Sci. Technol.* **9**, 239 (1972).

A. Y. CHO and F. K. REINHART, Growth of three-dimensional dielectric waveguides for integrated optics by molecular-beam–epitaxial method. *Appl. Phys. Lett.* **21**, 355 (1972).

A. Y. CHO and M. B. PANISH, Magnesium-doped GaAs and $Al_xGa_{1-x}As$ by molecular beam epitaxy. *J. Appl. Phys.* **43**, 5118 (1972).

1973

M. I. ABDALLA, D. B. HOLT and D. M. WILCOX, Epitaxial growth and structure of CdS films evaporated onto Ge. *J. Mater. Sci.* **8**, 590 (1973).

J. R. ARTHUR, Adsorption of Zn on GaAs. *Surf. Sci.* **38**, 394 (1973).

L. L. CHANG, L. ESAKI, W. E. HOWARD and R. LUDEKE, The growth of a GaAs–GaAlAs superlattice. *J. Vac. Sci. Technol.* **10**, 11 (1973).

L. L. CHANG, L. ESAKI, W. E. HOWARD, R. LUDEKE and G. SCHUL, Structures grown by molecular beam epitaxy. *J. Vac. Sci. Technol.* **10**, 655 (1973).

A. Y. CHO, Germanium doped epitaxial films by the molecular beam method. U.S. Patent no. 3,751,310 (1973).

C. T. FOXON, Molecular beam epitaxy. *Acta Electron. (France)*. **16**, 323 (1973).

J. L. KENTY, Physical vapor deposition of GaAs on single crystal sapphire. *J. Electron. Mater.* **2**, 239 (1973).

R. LUDEKE, L. L. CHANG and L. ESAKI, Molecular beam epitaxy of alternating metal–semiconductor films. *Appl. Phys. Lett.* **23**, 201 (1973).

J. W. MAYER, J. F. ZIEGLER, L. L. CHANG, R. TSU and L. ESAKI, Profiling of periodic structures (GaAs–$Ga_xAl_{1-x}As$) by nuclear backscattering. *J. Appl. Phys.* **44**, 2322 (1973).

P. D. SUDLOW and I. J. SAUNDERS, Molecular beam growth of gallium phosphide. *Phys. Status Solidi* A, **16**, K147 (1973).

J. C. TRACY, W. WIEGMANN, R. A. LOGAN and F. K. REINHART, Three-dimensional light guides in single-crystal GaAs–$Al_xGa_{1-x}As$. *Appl. Phys. Lett.* **22**, 511 (1973).

W. H. WEBER, E. M. LOGOTHETIS, H. HOLLOWAY, D. K. HOHNKE, A. J. VARGA and K. F. YEUNG, Thin-film IV–VI compound diode lasers. *J. Vac. Sci. Technol.* **10**, 289 (1973).

1974

J. R. ARTHUR, Surface stoichiometry and structure of GaAs. *Surf. Sci.* **43**, 449 (1974).

L. L. CHANG, L. ESAKI and R. TSU, Resonant tunneling in semiconductor double barriers. *Appl. Phys. Lett.* **24**, 593 (1974).

A. Y. CHO, Optical devices utilizing single crystal GaP or GaAs films epitaxially grown on CaF_2 substrates and method of fabricating source. U.S. Patent no. 3,830,654 (1974).

A. Y. CHO and H. C. CASEY, Properties of Schottky barriers and p–n junctions prepared with GaAs and $Al_xGa_{1-x}As$ molecular beam epitaxial layers. *J. Appl. Phys.* **45**, 1258 (1974).

A. Y. CHO and F. K. REINHART, Interface and doping profile characteristics with molecular beam epitaxy of GaAs: GaAs voltage varactor. *J. Appl. Phys.* **45**, 1812 (1974).

A. Y. CHO, C. N. DUNN, R. L. KUVAS and W. E. SCHROEDER, GaAs IMPATT diodes prepared by molecular beam epitaxy. *Appl. Phys. Lett.* **25**, 224 (1974).

A. Y. CHO and H. C. CASEY, Jr., GaAs–$Al_xGa_{1-x}As$ double-heterostructure lasers prepared by molecular-beam epitaxy. *Appl. Phys. Lett.* **25**, 288 (1974).

A. Y. CHO and M. B. PANISH, Molecular beam epitaxy method for fabricating magnesium doped thin films by group III–V compounds. U.S. Patent no. 3,839,084 (1974).

R. DINGLE, W. WIEGMANN and C. H. HENRY, Quantum states of confined particles in very thin $Al_xGa_{1-x}As$–GaAs–$Al_xGa_{1-x}As$ heterostructures. *Phys. Rev. Lett.* **33**, 827 (1974).

L. ESAKI, Computer-controlled molecular beam epitaxy. *J. Japan Soc. of Appl. Phys.* **43**, 452 (1974).

L. ESAKI and L. L. CHANG, New transport phenomenon in a semiconductor superlattice. *Phys. Rev. Lett.* **33**, 495 (1974).

R. F. C. FARROW, Growth of indium phosphide films from In and P_2 beams in ultra high vacuum. *J. Phys.* D, July 1974.

M. ILEGEMS and R. DINGLE, Acceptor incorporation in GaAs grown by beam epitaxy. *Proc. Symp. GaAs and Related Compounds, Deauville, France*, 1974.

R. LUDEKE, L. ESAKI and L. L. CHANG, $Ga_{1-x}Al_xAs$ superlattices profiled by Auger electron spectroscopy. *Appl. Phys. Lett.* **24**, 417 (1974).

R. LUDEKE and L. ESAKI, Electron energy-loss spectroscopy of GaAs and Ge surfaces. *Phys. Rev. Lett.* **33**, 653 (1974).

D. L. SMITH, Molecular beam epitaxy of II–VI compound waveguides, ARPA Contract no. N00014-73-0280 Reports of March 25, 1974 and June 30, 1974.

H. HOTTMAN and M. SCHULZ, Reflection splitting in RHEED investigations of vacuum evaporated GaAs layers. *Kristall Tech.* **9**, 45 (1974).